MICROFABRICATED DEVICES FOR DIRECT MEASUREMENTS OF QUANTAL TRANSMITTER RELEASE FROM LIVING CELLS

A Dissertation

Presented to the Faculty of the Graduate School

Of Cornell University

in Partial Fulfillment of the Requirements for the Degree of

Doctor of Philosophy

by

Brian Namghi Kim

January 2013

MICROFABRICATED DEVICES FOR DIRECT MEASUREMENTS OF QUANTAL TRANSMITTER RELEASE FROM LIVING CELLS

Brian Namghi Kim, Ph.D.

Cornell University 2013

Neurotransmitters are released in packets or quanta from vesicles that fuse with the cell membrane. The machinery proteins called Soluble N-ethylmaleimide-sensitive factor Attachment Protein Receptor (SNARE) proteins are known to mediate the vesicle fusion. The quantal release of neurotransmitters from fusion of single vesicles can be monitored using an electrochemical electrode by the oxidation of neurotransmitters which cause a transfer of electrons into the electrode. The resulting oxidation current reveals amperometric spikes that provide information about the frequency of release events, the number of released transmitter molecules from a single vesicle (quantal size) and the kinetics of quantal release events. While carbon fiber electrode (CFE) is most widely used as an electrochemical electrode, microfabricated planar electrodes made of platinum or gold are being developed as a more convenient way to interface with cells. Also, large arrays of planar electrodes can be easily fabricated, which enable high-throughput recording from living cells. In this dissertation, microfabricated devices for direct measurements of transmitter secretion from living cells are introduced.

Sensing electrodes can be fabricated on the surface of complementary metal–oxide–semiconductor (CMOS) integrated circuits (IC), which incorporate all the essential signal processing circuits in the chip. Such post-processing of CMOS chips is called post-fabrication. Using IC technology and post-fabrication, an electrochemical sensor array was developed that is capable of 100 parallel recordings. The IC sensor array was able to directly interface with living chromaffin cells to measure the quantal release of neurotransmitter. The biosensor was capable of resolving small (0.7 pA) and fast amperometric spikes

reporting release from individual vesicles. The effect of a Parkinson's disease drug called L-dopa was tested using the IC biosensor. The amperometric recordings of L-dopa treated cells revealed an increase in the amount of neurotransmitters release per vesicle by 73% which agrees with the known effect of L-dopa. An alternative and improved post-fabrication technique called tape-off is demonstrated in the following chapter. Tape-off is a dry and self-aligning method, which does not rely on photolithography for microfabrication and exhibits an excellent production yield and time reduction. Post-fabricated biosensor arrays with up to 320 electrodes exhibited stable performance with an electrolyte in contact and successfully measured oxidation of dopamine molecules. Measurement of quantal neurotransmitter release from living cells using the biosensor array fabricated using the tape-off method was demonstrated. Other potential applications of this new technique are discussed. In chapter 4, a portable and cost effective data acquisition system for the IC biosensor is presented that incorporates analog-to-digital converters (ADCs) and universal serial bus (USB)-communication. This data acquisition system outperforms other commercially available ADCs and allows the portable operation of the IC biosensor as it is fully powered through the USB connection. The functionality of the complete system was validated by measuring and storing dopamine oxidation data from the IC biosensor array. Finally, the use of a conducting polymer, poly(3,4-ethylenedioxythiophene) doped with poly(styrene sulfonate) (PEDOT:PSS), is used as detecting electrode material is demonstrated. Various architectures were evaluated to optimize the performance of PEDOT:PSS microelectrodes in direct contact with electrolyte and cells and the successful recording of the neurotransmitter oxidation released from chromaffin cells is shown. This result represents a new capability for organic electronics that could lead to devices that interface nervous system in novel ways with unique properties of polymer such as softness.

BIOGRAPHICAL SKETCH

Brian was born in Allentown, PA, being the youngest son of Sung June Kim and Eun Hi Lee with an older brother, Albert. He spent most of his childhood in Seoul, South Korea, and found his fondness to physics and math in school. He was heavily influenced by his father who didn't exclude his sons from the lectures about the landscape of his field, Biomedical Engineering, at the dinner table. He majored in Electrical and Computer Engineering at Hanyang University, Seoul, especially finding the subject of electronic circuits and semiconductor fabrication very interesting. Upon graduation, he wanted to contribute to the instrumentation of biophysical and biomedical research using his knowledge and talent in electronics. He joined Ph.D. program of Biophysics at Cornell University in 2008. After a year at Cornell, he married to Su In Lee and after two years, they gave birth to their daughter, Ara Bella. Unexpectedly, in the year (2011) of conception and birth of Ara, he made the most progress in the thesis project, which had been yet to function, and acquired notable results in the lab. During his study at Cornell, he developed a novel method to directly interface living cells with CMOS Integrated Circuits. Also he contributed in developing transparent and conducting-polymer electrodes to study exocytosis from endocrine and neuronal cells.

ACKNOWLEGMENTS

As Ph.D. program is long and being away from home for the first time was tough, I express my gratitude to every individual who helped me stay motivated and get use to the life in Ithaca.

At Cornell University, I am thankful to Prof. Manfred Lindau for inviting me into his lab and teaching me how to think critically. In Lindau research lab, Qinghua Fang and Ying Zhao kept the lab interesting and often gave me very helpful advices on my project. Joan Lenz kept the lab lively and helped me stay motivated. I am especially grateful to Kassandra Kisler, who taught me the basics of amperometry and helped me getting used to all the little details of scientific lab. Adam Herbst was a good friend who kept me accompanied at the toughest year. I also thank my special committee members, Prof. Barbara Baird and Prof. William Brown, and Prof. Bradley Minch for helpful discussions and guidance.

In Ithaca, I am particularly indebted to Prof. Elmer Ewing, Marilyn Ewing, and the rest of Ewing family. Elmer and Marilyn spent almost all the Sunday evenings listening to my boring personal stories and gave me such important advices on all the matters that went through my life in Ithaca. Also, they were always there for me when I needed help, even though not once I could do the same for them. With the Ewings, I felt like home and safe in Ithaca and was able to pursue Ph.D. till the end.

Lastly but most, I thank all my family members, my parents, Sung June Kim and Eun Hi Lee, my brother, Albert Dongghi Kim, and my wife and my daughter, Su In Lee and Ara Bella Kim. My parents were able to put me on the right track after countless failures, and they taught me to have positive attitude toward life which helped me in every way during the graduate study. I do recognize that I am privileged with a professor father and a very intelligent mother, although I don't always admit it. Albert was sometimes an inspiration and other times, a good friend who was fun to talk to. For my wife, Su In, I cannot thank her enough for all the sacrifices and dedications she made for me. I do not take any part of her sacrifices for granted and appreciate the fact that she decided to leave everything behind to help and support me. I was

only able to go through this difficult and tough period of my life in the presence of her support. To my precious daughter, Ara, she was a consistent source of joy. I am so much happier with her presence and having to think of her gave me the energy to work for that extra hour or two on very exhausting days.

TABLE OF CONTENTS

Biographical sketch iii

Acknowlegments iv

Table of contents vi

List of figures ix

List of abbreviations xi

1. Introduction 1

1.1. Vesicle secretion from living cells 1

1.2. Manipulating neurotransmitter secretions 2

1.3. Single-cell amperometry 3

1.4. Fabrication of planar electrodes to detect vesicle secretions 6

1.5. Integrated circuit for high-throughput amplifications and data processing 8

2. Parallel recording of neurotransmitters release from chromaffin cells using 10 × 10 CMOS IC potentiostat array with on-chip working electrodes 10

2.1. Abstract 10

2.2. Introduction 11

2.3. Material and methods 13

2.3.1. CMOS fabrication 13

2.3.2. Post-fabrication of Pt electrodes 14

2.3.3. Packaging 15

2.3.4. Solutions and DA application 17

2.3.5. Cell preparation and culture on the biosensor 17

2.3.6. Electrochemical recording, data acquisition and analysis 18

2.4. Results 19

2.4.1. Amperometric amplifier array 19

2.4.2. Multiplexing outputs from a large number of parallel acquisitions 19

2.4.3. Device validation by dopamine sensing 22

2.4.4. Amperometric recoding of transmitter release 25

2.5. Discussion 28

2.6. Conclusions 30

2.7. Notes to Chapter 2 31

3. Tape-off: an improved post-fabrication for high throughput biosensor array with 320 electrode array. 33

3.1. Abstract 33

3.2. Introduction 33

3.3. Results 34

3.4. Conclusion and Discussion 39

3.5. Material and methods 41

3.6. Note to Chapter 3 41

4. Portable data acquisition system for high throughput recordings 42

4.1. Introduction 42

4.2. Results 42

4.3. Material and methods 48

4.4. Conclusion and discussion 48

5. Conducting polymer microelectrodes to directly measure neurotransmitter release from single living cells 50

5.1. Abstract 50

5.2. Introduction 50

5.3. Material and methods 52

5.3.1. Fabrication of PEDOT:PSS microelectrodes 52

5.3.2. Cell preparation, electrochemical recording and analysis 54

5.4. Results 55

5.5. Conclusion and discussion 60

5.6. Note to Chapter 5 61

6. Conclusions and future directions 62

Bibliography 66

LIST OF FIGURES

1.1. Membrane fusion model 2

1.2. Electrochemical detection of neurotransmitter 4

1.3. Amperometric spike and parameters..... 5

1.4. Cell-measurement setups for CFE and planar electrode 7

2.1. Amperometric amplifier array 13

2.2. Packaging of the amperometric chip and live-cell experiment procedure..... 16

2.3. Time-division multiplexing of amperometric current measurements from 10 sensors in a column ... 21

2.4. Electrochemical recordings from the 100 electrodes array..... 23

2.5. Live chromaffin cell recordings of neurotransmitter release 26

2.6. The effect of L-dopa on quantal size revealed by IC biosensor..... 27

3.1. Post-fabrication using tape-off..... 35

3.2. X-ray analysis of patterned surface after tape-off..... 36

3.3. Photograph of resulted pattern on IC sensor and adhesive tape used for tape-off..... 37

3.4. Current measurements of dopamine (DA) oxidation under electrolyte contact 38

3.5. Live-cell measurement of the 320 electrode array post-processed by tape-off 39

4.1. USB-communicating ADCs and the functioning blocks on PCB 44

4.2. The portable recording setup using USB-ADC and the dopamine recording 46

4.3. The comparison of specifications and cost of different USB-ADCs 47

5.1. Cell interfacing PEDOT:PSS microelectrode and architectures 52

5.2. Amperometric recording of living cells using PEDOT:PSS electrodes 55

5.3. An amperometric trace recorded with a PEDOT:PSS microelectrode of type 3 57

5.4. Analysis of amperometric spikes from chromaffin cell with PEDOT:PSS and Pt microelectrodes ... 59

LIST OF ABBREVIATIONS

ADC ..... Analog to Digital Converter

CFE ..... Carbon-Fiber Electrode

CMOS ..... Complementary Metal–Oxide–Semiconductor

DA .....Dopamine

ECD.....Electrochemical Detector

EDX ..... Energy-dispersive X-ray Spectroscopy

IC..... Integrated Circuit

MCU..... Microcontroller

PCB ..... Printed Circuit Board

PEDOT:PSS ..... poly(3,4-ethylenedioxythiophene) doped with poly(styrenesulfonate)

SNARE.....Soluble N-ethylmaleimide-sensitive factor Attachment Protein Receptor

TIRF ..... Total Internal Reflection Fluoresence

USB ..... Universal Serial Bus

VIA..... Vertical Interconnect Access

XOP..... (Igor) External Operation

CHAPTER 1

INTRODUCTION

1.1. Vesicle secretion from living cells

Exocytosis refers to vesicle-membrane fusions that result in release of vesicle inner contents, such as neurotransmitters, to extracellular space. The vesicle secretion is an essential part of cell-to-cell communications. In neuronal networks, neurons transmit the excitation to the next neuron by the neurotransmitter release at synapses [1]. In the endocrine system, the adrenal gland secretes epinephrine (adrenaline) and norepinephrine (noradrenaline) into the blood vessel to affect multiple organs through systemic circulations [2]. The fusion of two lipid bilayer membranes requires significant amount of energy and rarely occurs spontaneously.

The key machinery that drives the membrane fusion is known to be the SNARE (Soluble NSF Attachment Protein REceptor) protein complex. The SNARE complex consists of 3 proteins: one synaptobrevin, one syntaxin, and one SNAP-25 (Synaptosomal-associated protein 25). Before the membrane fusion, synaptobrevin is located in the vesicle membrane and syntaxin with SNAP-25 is bound to the plasma membrane [3]. The details of how SNARE proteins deliver the energy to overcome the barrier and how lipids are arranged during fusion are still unknown. However, several studies suggested the possibility that the energy is produced as SNARE proteins zipper up into a continuous coiled coil, [4] known as “cis”-SNARE complex. In Fig. 1.1, this model of the membrane fusion process is shown. The process is initiated by the docking & priming of a vesicle to the plasma membrane. In this fusion model, SNARE proteins binds at their N-termini initially In this intermediate state, SNARE proteins form a “trans”-SNARE complex bridging two membranes. As the SNARE complex zippers up further towards C-terminus, an initial aperture is formed called the fusion pore. SNARE proteins are not fully zippered at this stage but a small amount of transmitter can leak out through the fusion pore. This is followed by a rapid expansion of the aperture, resulting in a flushing out of neurotransmitters to extracellular space.

After the fusion, the transmembrane domains of the SNARE proteins are located in a single membrane and this state is called “cis”-SNARE complex.

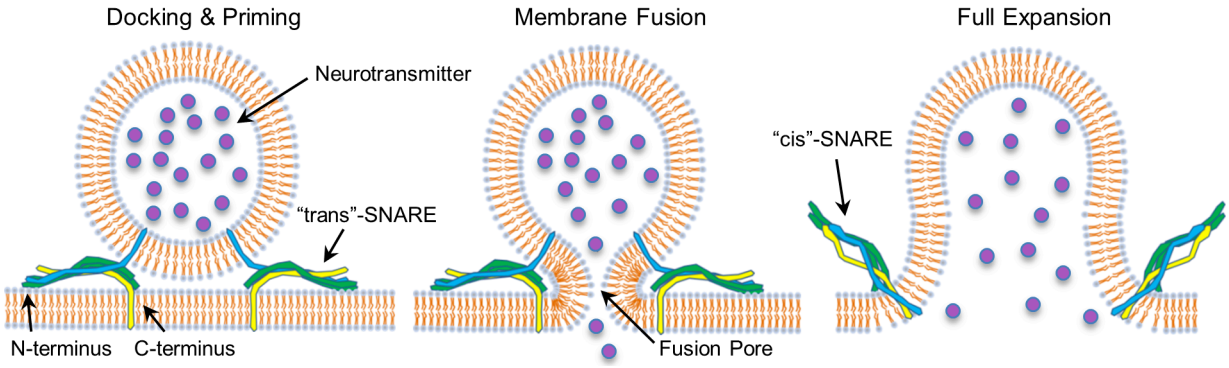

Figure 1.1. Membrane fusion model. In docking & priming step, the vesicle adheres to the plasma membrane. After an unknown time period, the membrane fusion begins as C-terminus of SNARE proteins come close together. Through the fusion pore, a small amount of neurotransmitter leaks out.

1.2. Manipulating neurotransmitter secretions

The secretion of transmitters can be manipulated in various ways. The amount of catecholamine release can be altered by treatment with certain types of drugs. For example, L-dopa is a drug for Parkinson’s disease treatment that increases the amount of transmitter molecules in each vesicle. Conversely, reserpine is a drug known to decrease the amount [5]. The frequency and dynamics of vesicle fusion events can be altered by direct modifications of the SNARE complex using mutations or botulinum neurotoxins [6].

Studying these manipulations can lead to useful pharmaceutical or biological information on vesicular secretion. Understanding the effect of the drugs on the cellular level, may help us evolve ideas how to affect a whole organism. Drugs with known effects on the transmitter release have been used to treat medical conditions such as Parkinson’s disease and hypertension [7]. To understand the dynamics of SNARE proteins during fusion, molecular manipulations such as specific SNARE protein mutations or neurotoxins can be applied to impair or enhance interactions between SNARE proteins. Comparing the

altered SNARE to wild type SNARE provides important clues on the molecular determinants of fusion dynamics. For example, SNAP-25 altered by Botox (Botulinum Toxin A) treatment exhibited significantly altered vesicle fusion efficiency and kinetics [8]. As the role of Botox is known to cleave the C-terminus of SNAP-25 [9], the altered fusion suggests the role of SNAP-25 C-terminus in normal fusion events. Genetic mutations can target certain bindings between SNAREs and allow researchers to understand SNAREs in the detail of single amino acid.

1.3. Single-cell amperometry

Membrane fusion can be observed using several different methods. Depending on the cell type, the size of vesicles can be on the order of ~40 nm to several hundred nm diameter and details of the fusion process are difficult to see under a light microscope. Thus, electron microscopy (EM) was adapted to reveal the physical appearance of exocytosis, but this does not offer the dynamics of fusion because the samples are no longer alive. In order to capture the dynamics in the membrane fusion, tools with fast time resolution were required. Fluorescence microscopy (FM) can offer relatively fast time resolution (~100 ms) and is thus used often to study membrane fusion [10]. However, the vesicle fusions occur in time scale of ~1 ms and cannot be seen in detail with FM methods. Single-cell amperometry is an indirect method to capture the dynamics of fusion with sub-ms time resolution Rather than looking at the fusion directly, amperometry is an electrochemical method to measure oxidizable neurotransmitters released to the extracellular space [11]. The schematics of amperometric neurotransmitter detection and recording are shown in Fig. 1.2. Neurotransmitters such as dopamine, epinephrine, norepinephrine, and serotonin are electroactive, and go through oxidation as they make contact with the electrode held at 700 mV potential (Fig. 1.2a). Each neurotransmitter molecule releases two electrons, as they are oxidized at the electrode and produce a flux of electrons into the electrode. This can be monitored using a current-to-voltage amplifier which converts small current (flux of electrons, $I_{oxidation}$) to high enough voltages ($V_{oxidation}$) that

can be recorded using analog-to-digital converters (Fig. 1.2b). Because the outgoing flux of neurotransmitter release reflects the fusion dynamics, the current measured using single-cell amperometry offers insights to the vesicle fusion.

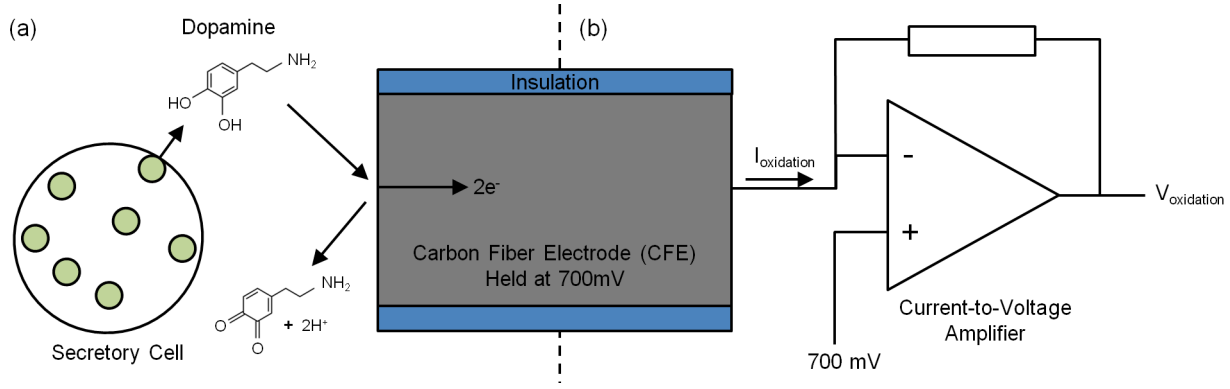

Figure 1.2. Electrochemical detection of neurotransmitter. (a) Dopamine released from a secretory cell is oxidized as it makes contact with carbon fiber electrode held at 700mV, which release 2 electrons per molecule. (b) The flux of electrons as many dopamine molecules oxidize is converted to voltage using a current-to-voltage amplifier.

For single-cell amperometry a carbon-fiber electrode (CFE) is most widely used. A CFE held at 700 mV is positioned to make contact with the secretory cell. Because the spontaneous release of vesicles is infrequent, cells are stimulated by ejecting high K^+ solution using a glass pipette aiming at the cell. The high K^+ concentration introduced at the surface of the cell depolarizes the membrane potential and this leads to the opening of voltage-gated calcium channels. The influx of calcium into the cell results in the removal of fusion inhibition which then triggers vesicle fusions. Fig. 1.3 shows an exocytotic event recorded using amperometry, a current spike that corresponds to a single vesicle release from a chromaffin cell [11]. Before the fusion of membranes, only a small background current is present because none of the neurotransmitter established contact with the electrode for oxidation. During fusion pore formation, a small increment of current is observed which is called a foot signal [12]. The foot current reflects the small leakage of neurotransmitter through the fusion pore (~ nm wide) which is formed at the very beginning phase of exocytosis [13]. This is followed by the steep increment of current as fusion pore

fully expands. The maximum current indicates the maximum flux of transmitter and it decays afterwards with the depletion of unoxidized transmitters.

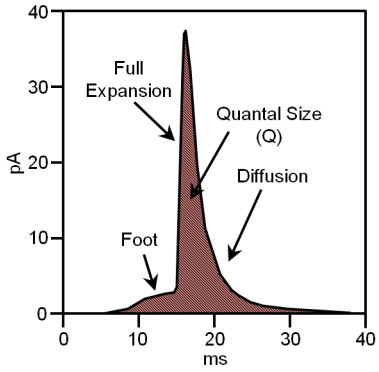

Figure 1.3. Amperometric spike and parameters. The full expansion that results in a steep increase of current is preceded by foot current that indicates neurotransmitters leaking through fusion pore. The spike is followed by the slow decay of current which is caused by the diffusion of neurotransmitters.

The area underneath the spike current is called quantal size (Q). Because each molecule transfers two electrons, the number ($N_{molecule}$) of molecules released from a specific vesicle can be calculated using the following conversion.

$$Q(t) = \int I_{oxidation} dt = zeN_{molecule} \quad \text{or} \quad N_{molecule} = \frac{Q(t)}{ze}$$

where z is the number of electrons transferred upon oxidation per molecule (z = 2 for catecholamine) and e is the elementary charge of an electron. The frequency of spikes in a unit time can be interpreted as how effective SNARE proteins are in driving membrane fusion, and foot duration and amplitude offer insights into the formation. the lifetime, and the structure of the fusion pore, respectively.

To determine the effect of molecular manipulations on the fusion process in living cells, single-cell amperometry is applied to characterize the change in amperometric events. As described above, the properties of exocytotic events such as quantal size, half-width, and foot are quantified for comparison. However, amperometric spikes vary in their properties, such as half-width, foot signal, and amplitude,

from cell to cell even when they are measured from the same cell type under the same condition. According to a previous study [14], it is more appropriate to use samples of mean spike values for individual cells and subsequently calculating the mean of the mean values from several cells, rather than to use averaging of individual spike values for comparison of experimental groups. Because spike values from one cell become one sample, the determination of the alteration requires a large number of single-cell measurements for the statistical analysis, regardless of how many events were detected for each individual cell. The significance in the difference between the biased group and control group is established by using student t-test which compares the Gaussian distribution of each group and indicates the likelihood that the experimental manipulation altered the fusion process.

1.4. Fabrication of planar electrodes to detect vesicle secretions

In order to perform single-cell amperometry, the electrode should be similar in size to the cells. Carbon-fiber electrode is a microelectrode that has the active electrode area of 20-80 μm^2. One of the reasons why CFE is widely used is that the fabrication of CFEs is simple and does not require very expensive equipment. For CFE fabrication, a single carbon-fiber is inserted in a glass capillary. Then it is pulled using a pipette puller which produces two CFE with carbon-fiber still connected. The carbonfiber is separated using scissors. The tip of each CFE is dipped in melting wax for few seconds and the wax is cured until it became solid. Finally, an active electrode area is produced by cutting the tip of CFE using a blade. Despite the simplicity of its fabrication, CFE recordings are inappropriate for high-throughput recordings. This is because the fabrication method is inappropriate for manufacturing electrodes in large numbers and also because each CFE requires a micromanipulator to position it precisely to the cell during experiments.

For a large scale fabrication of amperometric electrodes, microfabrication techniques can be used [15], which is often used in semiconductor fabrication. The microfabricated electrode can be easily printed in

large quantities compared to the CFE fabrication, and can be combined with optical measurements such as TIRF (Total Internal Reflection Fluorescence) microscopy. The microfabrication is typically done using photolithography, which is an image printing method using photoresist and a photomask. In Fig. 1.4, the cell-measurement geometries for CFE and microfabricated electrodes using a transparent conducting material [10], indium tin oxide (ITO), are shown as an example of the planar electrode setup. For CFE recordings, a CFE is carefully placed in close proximity to a living cell using a micromanipulator for electrochemical detection of single fusion events (Fig. 1.4a). In contrast, with surface patterned electrodes, a cell is placed on the active electrode area to be measured by dropping suspended cells on the surface. With the surface having a large array of ITO electrode repeats (not shown in the figure), the chance of suspended cells landing on the active electrode well-aligned is sufficiently high. The patterned ITO except the active area is insulated using photoresist to reduce unnecessary noise.

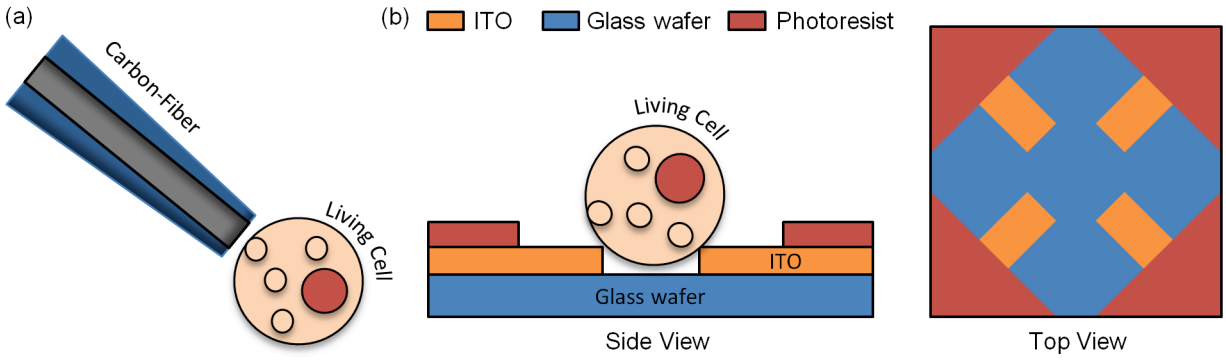

Figure 1.4. Cell-measurement setups for CFE and planar electrode. (a) CFE placed on top of the living cell for electrochemical detection. (b) A side and top view of ITO electrode array. On the glass wafer, transparent conductor ITO is patterned using microfabrication techniques. The patterned ITO is then insulated using photoresist except for the active area for detection. The living cell is placed on the ITO electrodes, showing the cell-measurement setup for planar electrodes. The top view shows an array of 4 ITO electrodes on the glass surface and the insulation of photoresist.

The electrode produced using microfabrication can be integrated with FM [10, 15]. Electrodes fabricated using transparent materials such as ITO can be integrated with TIRF microscopy, which is a FM technique using evanescent wave to excite fluorophores at the surface above the glass coverslip [10]. The

excitation light produced by TIRF has very limited penetration depth, and thus creates very thin layer of fluorescence excitation (< 150nm) above the glass substrate and allows high signal-to-noise observation of activities at the cell membrane. With the integration of amperometric recording and TIRF, the precise location of vesicle release was correlated with the kinetic information collected by amperometry. With the advance of microfabrication and the variety techniques available, various materials from gold and platinum to conducting polymer can be used to fabricate electrochemical electrodes.

1.5. Integrated circuit for high-throughput amplifications and data processing

High-throughput amperometry requires not only a large number of electrodes but also respective current-to-voltage amplifiers to each electrode. There are practical limits on how many pairs of electrode and amplifier can be operated in a laboratory set-up based on the physical size and cost of amplifiers. Another limitation is the wiring of electrode amplifier connections. Each electrode-amplifier pair requires an interconnection and as the number of pairs increase, the wiring becomes a limiting factor of space. Thus, an alternative approach is needed to produce high-throughput amperometry. Integrated Circuit (IC) technology is commonly used for very-large-scale-integration of circuits and previously has been used to integrate amplifiers and signal processing circuits for biosensors [16-20]. IC technology is a microfabrication-based method and consists of multiple layers of metals and other structures to allow the integration of active components (transistors), passive components (resistor and capacitor), and interconnects into a small piece of silicone. IC technology is widely used to build computer chips, which can have the transistor density of millions in mm^2. The advantage of implementing this technique to build biosensor arrays is that very large numbers of amplifiers can be easily integrated into a small die to process and record many amperometric recordings in parallel. IC design requires knowledge of analog circuit design and detailed protocol to submit design for fabrication, but does not require any experience on microfabrication. The IC design to fabrication is typically done in the following steps: schematic

design of the chip, simulation of circuit based on the IC parameter of certain fabrication, physical layout of the circuit, DRC (Design Rule Checking) to confirm that layout does not violate design rules, LVS (Layout Versus Schematic) to compare the circuit of layout to schematic, and design submission for tapeout to IC fabrication foundry.

IC chips provided by the foundry are not adequate for a direct measurement application because active electrode materials cannot be fabricated under the foundry fabrication. Thus, an integration of the integrated electronic circuit and electrode array require a further modification using microfabrication techniques to pattern electrode materials on IC chips. The modification of IC chips by microfabrication is termed post-fabrication [21]. In this dissertation, improved post-fabrication methods are demonstrated. Using IC post-fabrication methods, the development of an integrated electrochemical sensor array with up to 320 electrodes has been achieved. The high-throughput measurements of quantal release events and the modulation of quantal size by the L-dopa treatment on chromaffin cells are demonstrated.

CHAPTER 2

PARALLEL RECORDING OF NEUROTRANSMITTERS RELEASE FROM CHROMAFFIN CELLS USING 10 × 10 CMOS IC POTENTIOSTAT ARRAY WITH ON-CHIP WORKING ELECTRODES

2.1. Abstract

Neurotransmitter release is modulated by many drugs and molecular manipulations. We present an active CMOS-based electrochemical biosensor array with high throughput capability (100 electrodes) for on-chip amperometric measurement of neurotransmitter release. The high-throughput of the biosensor array will accelerate the data collection needed to determine statistical significance of changes produced under varying conditions, from several weeks to a few hours. The biosensor is designed and fabricated using a combination of CMOS integrated circuit (IC) technology and a photolithography process to incorporate platinum working electrodes on-chip. We demonstrate the operation of an electrode array with integrated high-gain potentiostats and output time-division multiplexing with minimum dead time for readout. The on-chip working electrodes are patterned by conformal deposition of Pt and lift-off photolithography. The conformal deposition method protects the underlying electronic circuits from contact with the electrolyte that covers the electrode array during measurement. The biosensor was validated by simultaneous measurement of amperometric currents from 100 electrodes in response to dopamine injection, which revealed the time course of dopamine diffusion along the surface of the biosensor array. The biosensor simultaneously recorded neurotransmitter release successfully from multiple individual living chromaffin cells. The biosensor was capable of resolving small and fast amperometric spikes reporting release from individual vesicle secretions. We anticipate that this device will accelerate the characterization of the modulation of neurotransmitter secretion from neuronal and endocrine cells by pharmacological and molecular manipulations of the cells.

2.2. Introduction

The electrochemical recording of biomolecules has a wide range of applications: from biomedical sensing, with implanted electrodes in a living animal's brain to detect the level of dopamine (DA) release [22], to biophysical applications where it is used to understand the membrane fusion mechanism, called exocytosis, mediating neurotransmitter release [11, 12, 23-25]. Some neurotransmitters, such as DA, epinephrine (adrenaline), norepinephrine (noradrenaline), and serotonin, are oxidized by a polarizable electrode held at ~700mV vs. an Ag|AgCl reference electrode, and the resulting electron transfer is measurable using a current-to-voltage amplifier. Polarizable electrodes have high electrolyte/electrode interface resistance that introduces negligible background current. Thus, the oxidation (faradic) current can be closely monitored with high signal-to-noise ratio, a technique called amperometry. Neurotransmitters are released in packets or quanta from vesicles that fuse with the cell membrane, which can be detected as an amperometric spike [11, 12]. The amperometric spike provides the precise amount and time course of released molecules in a single vesicle fusion event and thereby details of the vesicle-plasma membrane fusion process. The total charge that is collected from a single vesicle release (quantal size) is closely related to the volume of the vesicle [13, 26-28], because the neurotransmitter concentration inside the vesicles is relatively constant [5, 29]. A so-called foot signal preceding the steep amperometric spike [12] indicates neurotransmitter leaking through a narrow fusion pore at the initial step of exocytosis [13, 30]. Based on this understanding of the biophysical mechanisms that determine the features of the amperometric spike, amperometry can be used to identify the effects of drugs on vesicle fusion in living cells. Amperometric recordings have revealed that quantal size is increased by the Parkinson's drug L-Dopa and decreased by drugs such as reserpine [23, 31, 32]. Alternatively, treatment with drugs such as botulinum toxin A (Botox) appear to influence the rate of release events, and the properties of the fusion pore, without affecting quantal size [6, 33].

Amperometric spikes vary in their properties, such as half-width, foot signal, and amplitude, from cell to cell even when they are measured from the same cell type under the same condition [14]. In order to identify the effect of a drug on secretory cells, a large number of single cell measurements must therefore be performed to determine statistical significance of a change in the mean value. Conventional amperometric recordings are performed with a carbon fiber microelectrode positioned close to a single cell using a micromanipulator under microscopic observation. Not only is the equipment costly, but an expert performing the cell recordings one by one will need to spend a long time to gather enough recordings to derive conclusions with statistical significance.

Such limitations may be overcome by development of a scalable electrochemical detector array in which the working electrodes are integrated with the amplifiers. Amplifier and sensor integration using CMOS technology has been used in different biosensing applications to reduce the size of the biosensor system but still sustain the high-quality performance of conventional systems [16-20]. For amperometric recordings of quantal release, a low-noise CMOS potentiostat using a shared amplifier structure has been developed [34] onto which suitable polarizable electrode materials can be deposited [21].

Here, we present an electrochemical biosensor array with a large number of electrode-amplifier pairs. This biosensor can simultaneously measure the quantal release of oxidizable transmitters from many cells cultured on-chip. The high-throughput capability provides a great benefit to both biomedical and biophysical applications. In biomedical implants, this biosensor could provide a spatially resolved image of a DA release. As a biophysical research instrument, its parallel amplifier circuit-electrode pairs would allow large numbers of single-cell recordings to be performed simultaneously. The application of high-throughput electrochemical sensors arrays will drastically accelerate the elucidation of the mechanisms of transmitter release and their modulation by drug treatments.

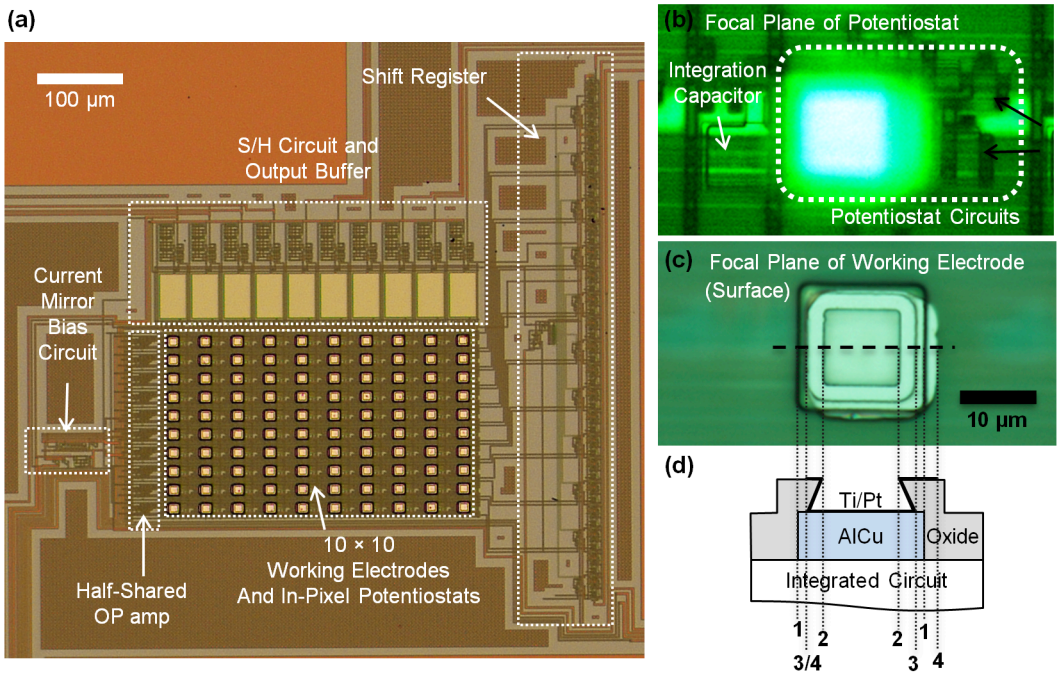

Figure 2.1. Amperometric amplifier array. (a) Photograph of chip surface with working electrodes and underlying circuitry after post-fabrication. The 10 × 10 electrode array was visible as bright squares; each electrode was 15 µm × 15 µm in size. Each in-pixel potentiostat contains only a half of an operational amplifier taking advantage of a half-shared operational amplifier design. The shift register controlled the timing of the S/H circuit to multiplex the electrode outputs per each column of 10 electrodes. (b) and (c) are microphotographs of individual electrode /potentiostat array element at different focal planes. The focal plane of (b) was at the underlying potentiostat, consisting of 9 transistors (two of which are indicated by black arrows) and an integrating capacitor that converted the recording current to voltage. The focal plane of (c) was at the surface working electrode above the potentiostat. (d) Schematic of electrode topology. 15 µm × 15 µm AlCu contacts served as interconnection between the surface patterned Pt electrode and the potentiostat. The overglass has 10 µm ×10 µm openings at the top with an undercut expanding to a ~12 µm × 12 µm area of exposed AlCu. The thick black line, atop AlCu and Oxide, indicates the area covered by Ti/Pt. The cross section along the horizontal dashed line is shown schematically in (c). The vertical dotted lines indicate the edges of the AlCu contacts (1), the overglass opening (2), the undercut (3), and the slightly misaligned bright area where Pt is patterned (4).

2.3. Material and methods

2.3.1. CMOS fabrication

The CMOS IC incorporating a 10 × 10 array of potentiostats as well as timing and readout circuitry (Fig. 2.1a) was designed in Tanner Tools EDA, simulated using H-Spice with parameters for On

Semiconductor C5F/N, and the design submitted for fabrication through MOSIS. The On Semiconductor C5F/N (previously known as AMIS 0.5 μm) process does not offer a polarizable electrode material such as gold or platinum among the options of metal layer materials. Therefore, 15 μm × 15 μm AlCu contacts were included in the design to serve as interconnection between the electrode material and the underlying integrated amplifier shown in Fig. 2.1b. Using a half-shared operational amplifier design [34], one potentiostat circuit consisted of only 9 transistors and one capacitor for the oxidation charge integration that is small enough to be positioned under an electrode. To deposit Pt directly onto these contacts, the design included 10 μm × 10 μm openings in the overglass layer in register with the AlCu contacts. Due to the aggressive etching process, these openings had an undercut structure as shown in Fig. 2.1c, d.

2.3.2. Post-fabrication of Pt electrodes

For the post-fabrication of the Pt electrodes each 3 mm × 3 mm die was attached to a 25 mm × 25 mm glass coverslip (VWR micro cover glass) with epoxy (DOUBLE/BUBBLE Epoxy, HARDMAN) to facilitate handling and to prevent damage by electrostatic discharge. After cleaning the surface of the IC and coverslip with acetone and isopropanol, positive photoresist S1813 (Shipley) was spin-coated onto the surface at 4000 rpm for 30 sec and baked on a hotplate at 90ºC for 1 minute. Using an ABM contact aligner and a negative toned mask, the pattern for the Pt electrodes was transferred to the photoresist on the IC by UV exposure. The die/coverslip was then placed in a YES Image Reversal Oven with ammonia gas, exposed to UV light for 60 s, and developed for 60 s in MF-321, which removed the photoresist where Pt would be deposited and left the photoresist elsewhere as a sacrificial layer. Following Pt deposition (see below) this sacrificial layer was removed (Photoresist Remover 1165) leaving the patterned Pt electrode array, with the surface between the electrodes insulated by the overglass layer.

Due to the undercut in the openings exposing the AlCu contacts unidirectional Pt vapor deposition resulted in imperfect coverage of the exposed AlCu contacts by Pt. As a consequence, electrolyte could

make low resistance contact with the AlCu, leading to excessive currents. To achieve complete coverage of the AlCu contacts, conformal electron beam physical vapor deposition of 15 nm titanium and 100 nm Pt was performed using a rotating shelf. This process introduced multiple angles of incidence to the incoming vapor of metal atoms, resulting in complete coverage of the AlCu contacts and created a continuous Ti/Pt layer at the side wall of the overglass openings as well as the sacrificial photoresist layer on top. To avoid the formation of rough edges of the Pt at the edges of the overglass openings during lift-off of the sacrificial layer, the openings in the photoresist defining the Pt covered areas were slightly larger (15 μm × 15 μm) than the overglass openings such that small defects at the edges of the Pt electrode would not impact the chip's performance. A schematic of the geometry with an aligned image of a single electrode of the array (Fig. 2.1c) is shown on an expanded scale in Fig. 2.1d.

2.3.3. Packaging

The die was mounted on a side-braze Dual in-line Package (Addison Engineering, San Jose, California, USA) using 5 Minute Epoxy (Devcon) and wire bonded (Fig. 2.2a). To prevent contact of the electrolyte with the contact pads and wire bonds, these areas were insulated with silicone (RTV 615, GE) (Fig. 2.2b). The chip carrier with the mounted die was placed on a heated metal block during the application of silicone accelerating the curing process to prevent flow of silicone to the center of the IC where the working electrodes must remain exposed for direct contact with cells and the electrolyte.

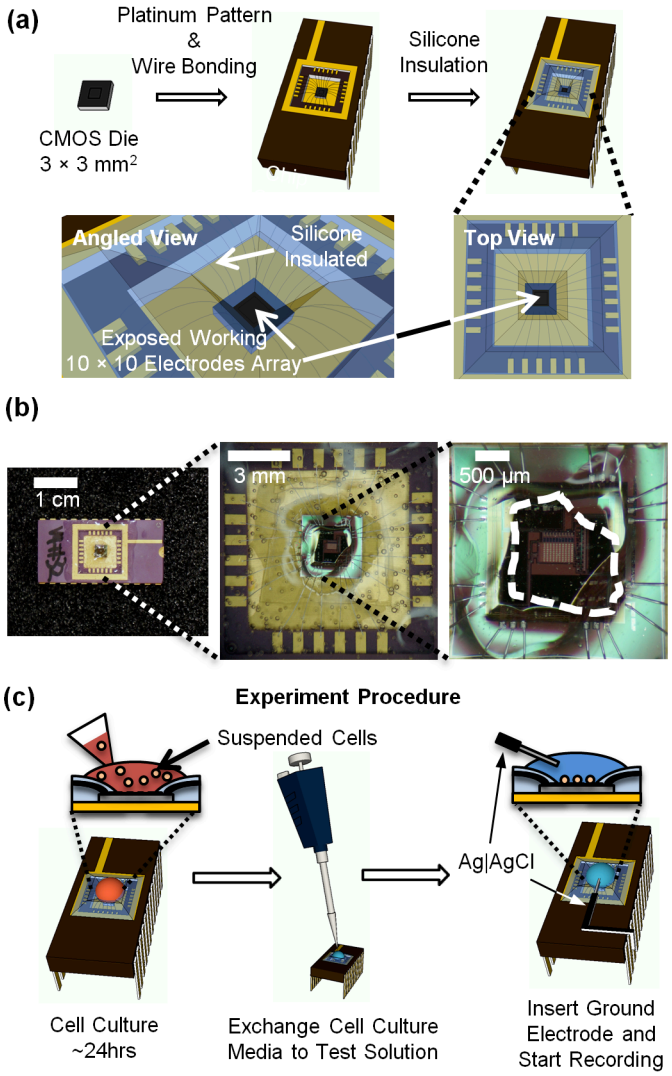

Figure 2.2. Packaging of the amperometric chip and live-cell experiment procedure. (a) A 3 × 3 mm^2 CMOS die with post-fabricated Pt electrodes was wire bonded to a chip carrier. Silicone was applied at the surface of the chip carrier insulating the wire bonds and contact pads. This only left the center of the CMOS die exposed where the working electrode array was located. (b) Photograph of IC biosensor package with silicone insulation of wire bonds and contact pads. The area of the IC that was exposed without silicone coverage is indicated by the white dashed line. The amperometric amplifier array shown in Fig. 2.1a was located at the center of this exposed area. (c) Schematically shown experiment procedure from the cell culture on the chip to the live-cell recording.

2.3.4. Solutions and DA application

The standard solution contained 140 mM NaCl, 5 mM KCl, 1 mM $MgCl_2$, 10 mM $CaCl_2$, and 10 mM HEPES/NaOH (pH 7.3) with the osmolality adjusted to 300 mmol/kg by adding glucose. The high K^+ stimulating solution contained 140 mM KCl, 5 mM NaCl, 1 mM $MgCl_2$, 10 mM $CaCl_2$, and 10 mM HEPES/NaOH (pH 7.3) with the osmolality adjusted to 300 mmol/kg by adding glucose. The electrode array was covered with 40-100 µL of standard solution and DA was injected from a pipette adding 10 µL of standard solution containing DA at high concentration (0.35-5.3 mM). For measurements of the DA concentration dependence, the electrode array was covered with 40-90 µL of the standard solution and 10 µL of DA solution was rapidly mixed into the solution to reach final concentrations of 350 nM, 3.5 µM, 35 µM, 70 µM, and 105 µM.

2.3.5. Cell preparation and culture on the biosensor

Bovine adrenal glands were obtained from a local slaughter house and chromaffin cells were cultured in 70 mL cell culture flasks as described [35]. After one day of incubation at 37°C and 10 % CO_2, the cells were suspended and plated on the Poly-D-Lycine (0.05%) coated biosensor (Fig. 2.2c). The biosensor array with the cell cultured was incubated for another ~ 24 hrs before recordings were made. Shortly before the recording, the cell culture media atop the biosensor was exchanged with 50 µL of the standard solution. For stimulation of neurotransmitter secretion, 50 µL of the stimulating solution was added to the standard solution, resulting in a final concentration of 70 mM of KCl.

For the L-dopa experiment, L-dopa was diluted in the standard solution to establish a concentration of 200 µM. The cells were cultured on the IC biosensor with the same method described above. An hour before the recording, the cell culture media on the IC biosensor was replaced with 200 µM L-dopa solution and again incubated. For the control group, the culture media was replaced with the standard

solution instead. Just before the experiment, the cells on IC biosensor were washed with the standard solution twice.

2.3.6. Electrochemical recording, data acquisition and analysis

After an Ag|AgCl reference electrode was inserted into the bath and connected to ground, power was supplied to the chip along with the clock signals. Initially, the potentiostat outputs were saturated due to the capacitive currents charging the electrode capacitance to 700 mV, followed by a slow decay to a very small stable baseline current within 1 min. The analog output signals were digitized by a 16-bit analog-to-digital converter (ADC) (PCI-6251 and PXIe-6368, National Instruments, Austin, TX) using Igor Pro 6, Wavemetrics for data acquisition and a user written procedure for de-multiplexing and data analysis. The time windows during which the signals from each electrode were presented at the output pins were 25 μs long and a sampling rate of 500 kS/s per output (column with 10 electrodes) was used to acquire the signals from all 10 columns (100 electrodes). When only one column of electrodes was recorded a sampling rate of 1 MS/s was used. The recordings were low pass filtered digitally in IGOR PRO by 5-s binomial smoothing for the DA injection experiments and by 10-ms binomial smoothing for the live-cell recordings. Data analysis for live-cell experiment was performed using Quanta Analysis software as described [36]. For the L-dopa experiment, a custom-modified version of Quanta Analysis software was used for data analysis. The modifications included a step of baseline subtraction before the analysis to assist the automatic spike detection to better tolerate larger baseline fluctuations. The number of events per electrode ranged from 3-20.

2.4. Results

2.4.1. Amperometric amplifier array

Amperometric detection of DA and other catecholamines is typically performed by a current measurement applying ~700 mV holding potential to a polarizable working electrode relative to an Ag|AgCl reference electrode that was inserted into the electrolyte and connected to ground. The array shown in Fig. 2.1a incorporated an array of potentiostats [34] connected to surface patterned Pt working electrodes and arranged in 10 rows × 10 columns.

DA molecules making contact with the electrode are oxidized, transferring two electrons per molecule to the electrode. The arrival of DA molecules thus produces an oxidation current that passes through the potentiostat circuit and is integrated on a 50-fF capacitor (C_{charge}, Fig. 2.3a) resulting in a voltage signal, V_n, which is read out every sampling period as a value V_{sn} at the end of the integration period. The faradic current from the oxidation of catecholamine molecules in individual release events from chromaffin cells [11] can be up to 500 pA in amplitude but foot signals indicating fusion pore properties [12] require a resolution of <10 pA. To resolve currents in this range, we have chosen an amplifier gain of ~10mV/pA. To resolve the time course of individual release events a sampling rate of 2 kS/s per electrode is typically used. The rms noise of the potentiostat is ~100 fA (Ayers et al., 2007), comparable to that of conventional low-noise amplifiers. In practice, conventional amperometric carbon-fiber electrodes act as antennas picking up excess noise, which is minimized in the microchip technology presented here, because the Pt electrodes are patterned directly on top of the IC.

2.4.2. Multiplexing outputs from a large number of parallel acquisitions

When a large number of parallel electrode-amplifier pairs were incorporated, the main challenge becomes to sample all the data in parallel and transfer them to a computer for storage and analysis. We

used a time-division multiplexing approach to limit the number of outputs from the chip to be sampled by the computer to 10 (1 per column), and staggered the integration periods for the capacitors along a column, so that, while one amplifier is being read out, all the other potentiostats in the column continue to integrate their respective input currents. Thus, each potentiostat integrated its input current for 95% of the sampling interval (475 µs/sample), interrupted by 25-µs readout and reset periods.

During the 475-µs integration interval, the oxidation current entering through the potentiostat decreased V_n as electrochemically transferred electrons fill C_{charge}. At the end of the sampling interval, the reset clock r_n goes low, resetting V_n to V_{DD} (Fig. 2.3b). The change in V_n at the end of the integration period (V_{sn}) represents the inverse of the total charge collected during 475-µs with an offset voltage of V_{DD}. The polarity of V_{sn} is reversed and the offset adjusted using capacitor C_{clamp} and the clamp switch. All the voltages $V_0..V_9$ are in parallel, such that the row selection signal r_{sn} carries V_n to C_{clamp}. At the end of the integration period, the clamp switch is closed by the high clamp signal (Fig. 2.3b, Clamp - gray line) to reset V_{clamp} to a default voltage, in this case 300 mV. At the time of the reset of V_n to V_{DD}, the Clamp clock goes low (gray line) to take V_{sn} to V_{clamp} such that the decrease in V_n over the 475 µs integration period is transferred to V_{clamp} as an increase. In this way, all outputs in a column are serially presented at a single output through time-division multiplexing (Fig. 2.3b dashed lines). V_{clamp} is read out through an output buffer to lower the output impedance. The IC was operated from a main clock (CLK, 40 kHz and 50% duty cycle) and a sampling clock (SCLK, 2 kHz and 95% duty cycle). From these clocks the timing circuitry in the IC derives the subclocks (Fig. 2.3c). As shown in Fig. 2.3c, SCLK enters a shift register, a series of D flip-flops, to produce the reset signals (i.e., $r_0,..., r_9$) for resetting each row's C_{charge} capacitor. The reset signals are identical to SCLK except for a delay of 2n (where n is the row number) times the 25-µs CLK period. As shown in Fig. 2.3c, a row selection signal for row n (r_{sn}) is generated using a two-input NAND gate whose inputs are r_n and Q_{2n} (i.e., the subclock that precedes r_n by a period of CLK).

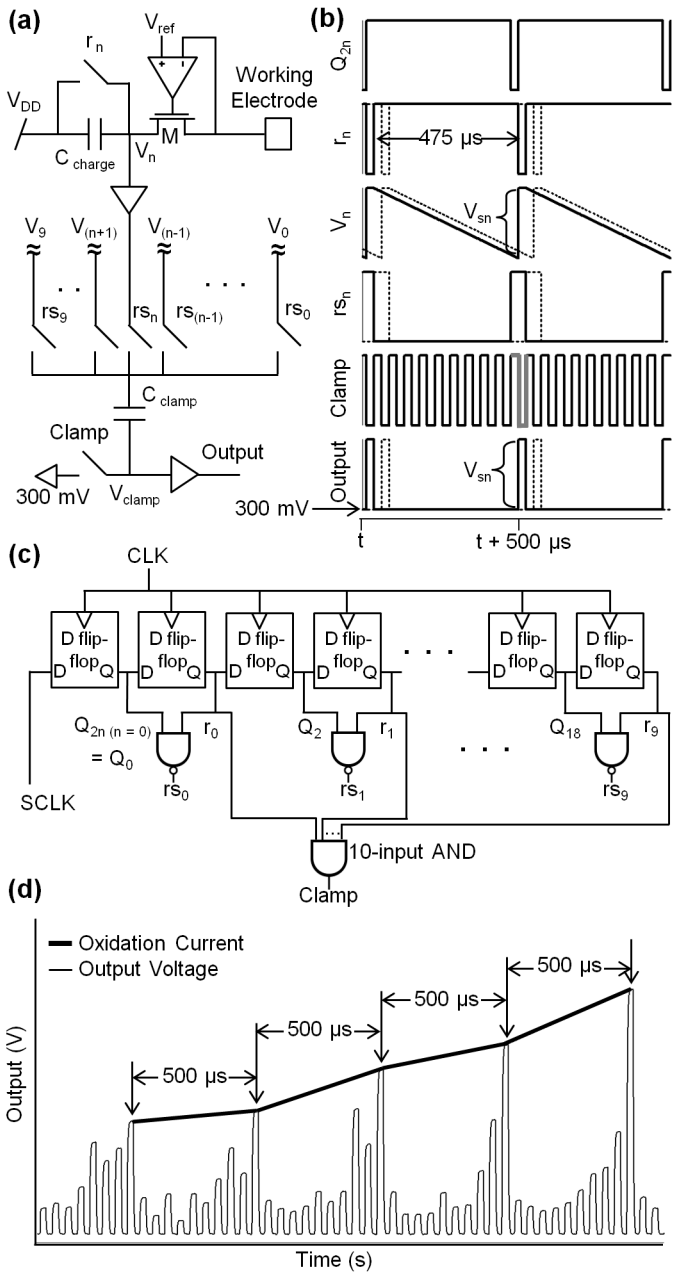

Figure 2.3. Time-division multiplexing of amperometric current measurements from 10 sensors (n=0…9) in a column. (a) Potentiostat circuit and multiplexer. The oxidation current at the working electrode charges C_{charge} decreasing V_n over the integration period, which is set to 475 µs by clock r_n that reset V_n back to V_{DD} (5V). At the end of integration cycle, rs_n switch closes and connects V_n to C_{clamp}. C_{clamp} is an AC coupling capacitor that removes the DC component in V_n, and is controlled by the on/off cycle of the Clamp switch. After this cycle, the $rs_{(n+1)}$ switch is closed and couples $V_{(n+1)}$ through C_{clamp} to the output. This is repeated to multiplex all the outputs in a time-division fashion. (b) Timing signals, time course of voltage V_n at C_{charge} and the final output signal V_{sn} representing the total amount of charge collected during the integration period. (c) Subclock generation timing circuit generates reset clocks (r_n), row selection clocks (r_{sn}) that is produced using Q_{2n} and r_n, and a clamp clock (Clamp). (d) Example output

from one column of electrodes, illustrating the de-multiplexing process. The output was recorded with a 1-µs sampling interval. The trace starts with the data from the electrode of row 0, followed by that of row 1, and so on. Extracting the values at the times indicated by arrows provides the time course of the current measured by the electrode in row 7 (thick black line).

An example stream of output data from an individual column is shown in Fig. 2.3d. Data from all 10 electrodes appear sequentially in a 500-µs time interval. The multiplexed output was de-multiplexed after sampling by the computer. In the current implementation the signal from row 0 was identified by recording SCLK and aligning it with the column output, using the known delay for each row selection (r_{sn}) relative to SLCK. The thick line in Fig. 2.3d illustrates the extraction of the signal V_{s7} as an example of output demultiplexing. It represents the time course of the current that was measured at the electrode located in row 7, with a sampling rate of 2 kS/s. Likewise the signals from all rows were extracted and saved separately for further analysis.

2.4.3. Device validation by dopamine sensing

DA is readily oxidized in amperometric recordings with surface patterned Pt microelectrodes [37] and the sensor array was tested measuring the electron transfer induced by DA application (Fig. 2.4a). Fig. 2.4b shows the current from an electrode in column 9 in response to DA addition to a final concentration of ~70 µM. The measured current level showed a slow increase after DA injection to ~120 pA reflecting the diffusional DA to the electrodes.

Application of DA at final concentrations of 350 nM, 3.5 µM, 35 µM, 70 µM, and 105 µM in the bath solution, produced oxidation currents at the 100 electrodes. The current change measured from each electrode was quantified by taking the difference between first and last point of 0.2 Hz smoothed recordings of 60 seconds duration. Data from all 100 electrodes were averaged to determine the average current change for each DA concentration. The average current of the 100 electrodes increased linearly with DA concentration in the range 3.5 – 105 uM with a slope of 1.20 pA/µM (Fig. 2.4c).

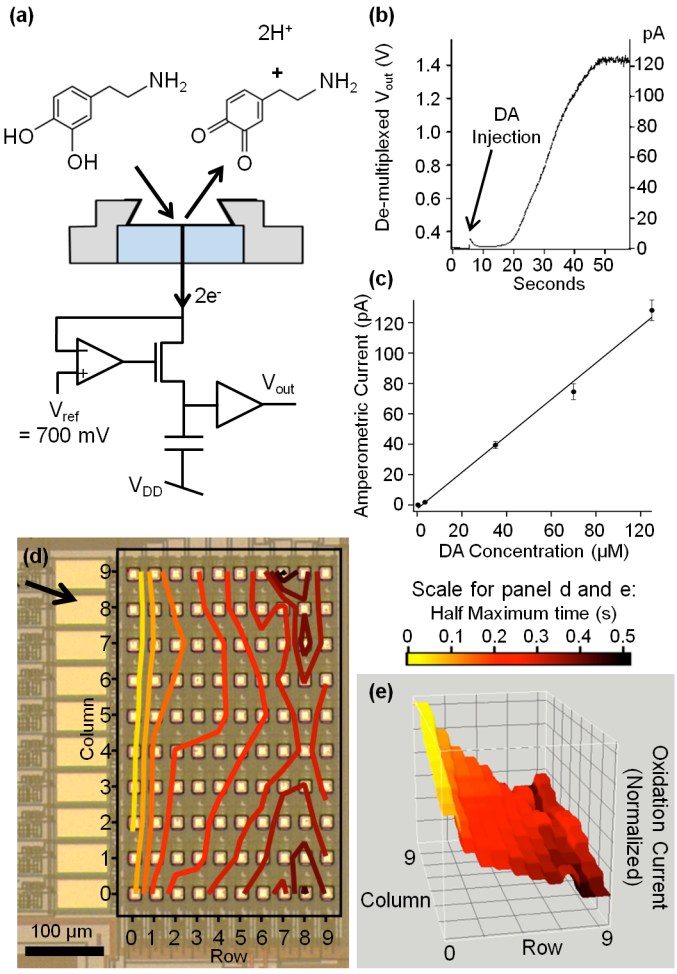

Figure 2.4. Electrochemical recordings from the 100 electrodes array. (a) Scheme of DA recording concept. At the surface of an electrode that is held at 700mV, a DA molecule making contact with the platinum through diffusion and is oxidized, transferring 2 electrons to the electrode and leaving DA-o-quinone to diffuse away. V_{out} changes as the charges that enter the electrode pass through the potentiostat circuit and are collected at the capacitor. (b) Oxidation current from an electrode initially covered with 40 µL of standard solution after injection of 10 µL standard solution containing 350 µM DA. (c) DA concentration dependence of average currents. Data points are averaged from all 100 electrode of the 10 × 10 electrode array. The error bars are SEM. The slope of linear fit was 1.20 pA/µM. (d, e) Representations of DA response from 100-electrode array. Following a single injection of DA, all electrodes reported oxidation currents and the half maximum times of the dopamine responses are plotted for every electrode according to its position. Time 0 was defined as the time where the electrode in column 9, row 0, was half saturated. (d) Photograph indicating the orientation of the electrode array and the direction of DA diffusion from the injection site (arrow). Colored contour lines indicate half maximum times of current at each electrode. (e) Three-dimensional DA concentration profile measured from all 100 electrodes simultaneously at t = 200ms. The z-axis is the normalized oxidation current measured from the electrode array to best visualize the diffusional wave of DA. Colors indicate half maximum times for individual electrodes as in (d).

The lowest concentration that we could reliably detect was 0.35 µM giving an average current of 0.1 ± 0.06 pA (s.d.). The average responses of the different electrodes in the array were 39.5 ± 23.2 pA (s.d.) in the presence of 35 µM and 128.2 ± 67.5 (s.d) in the presence of 105 µM DA. Such variability is presumably in part due to differences in area between the different electrodes but is in part also due to variations in DA concentration due to overlapping diffusion layers as has been shown for DA sensing by a passive carbon ring microelectrode array [38]. The calibration of amplifier gain was tested by direct current injection into the surface electrode (held at 700 mV) via a 10 GΩ resistor connected to ground for each of the 10 electrodes in a single column. The average from the 10 electrodes was 76.7 ± 2.6 pA s.d., indicating that the variability of gain between different electrodes is <3.5 %.

Corresponding measurements with two other biosensor arrays provided slopes of 0.95 and 0.90 pA/µM. These small variations are presumably due to the variations in the active size of the electrodes, which result from separate die-based post-fabrications. The variability will be reduced in wafer-based post-fabrication. It should be noted that the values of 0.95 and 0.90 pA/µM were obtained with two different devices on the same day with the same solutions, whereas the 1.2 pA/µM slope was obtained on a different day with a different freshly prepared DA solution. Given the instability of DA, differences in actual DA concentration may have contributed to the apparent differences in sensitivity.

The observed variability between electrodes and between different arrays does not affect the measurement of single vesicle release events because the individual release sites are in close contact with the sensor and have dimensions that are almost 100 times smaller than the electrodes ensuring complete oxidation of all released molecules.

The functionality of the full 100-electrode array was further demonstrated by injecting DA at a final concentration of ~500 µM, which eventually saturated the potentiostats. For a graphical representation of the electrode responses, the time where the current recorded by a particular electrode reached its half saturation value was coded in grey scale in Fig. 2.4d. Fig. 2.4e shows a contour plot of half saturation

times for the different electrodes of the array, visualizing the flow of DA over the surface of the electrode array. These plots indicate that DA molecules initially appeared at the upper left side of the electrode array. The electrode in column 9, row 0, showed the most rapid response, very closely followed by its neighboring electrodes as the DA diffused toward the lower electrodes. Fig. 2.4f shows DA concentration profile at t = 200ms showing the wave of DA reaching the electrodes and eventually saturating the potentiostats.

2.4.4. Amperometric recoding of transmitter release

To demonstrate the live-cell measurement of single vesicle release events, chromaffin cells were cultured on the biosensor for 24 hrs (Fig. 2.5). The chip provided stable baseline currents <100 pA after up to 3 days with cultured cells in the incubator, which corresponds to a nominal electrode resistance of 7 $G\Omega$. The chip provided stable currents after up to 3 days with cultured cells in the incubator. Typical cell sizes are < 20 μm but some cell aggregates of larger size are also present. Out of the 12 electrodes shown in Fig. 2.5, 8 electrodes were fully or partially covered by chromaffin cells. After a high K^+ stimulation, amperometric events were recorded by most of cell-covered electrodes as well as adjacent electrodes. Each amperometric spike corresponds to quantal release of the contents from a single vesicle and its integral is proportional to the number of released molecules (quantal size). In Fig. 2.5, the amperometric traces are plotted at the spatial locations of the respective electrodes. The electrode with a single cell atop (column 2 × row 3) recorded fast amperometric spikes with ~ 10 ms half-width. For this electrode, two spikes are shown on an expanded scale, one with 14.8-pA amplitude and 11-ms half-width and the other with 1.6-pA amplitude and 40-ms half-width which was the smallest spike recorded by this electrode. The quantal size ranged from 0.1 pC to 1.2 pC with an average of 0.49 pC These values agree well those previously reported for carbon-fiber experiments on bovine chromaffin cells [11, 12], indicating that the sensor readily detects the released molecules. With 2 electrons transferred per molecule, a quantal size of

0.1 pC corresponds to ~300,000 molecules. The noise in the recordings was ~0.15 pA rms at 100 Hz bandwidth. We estimate that release events down to ~6000 molecules should be detectable.

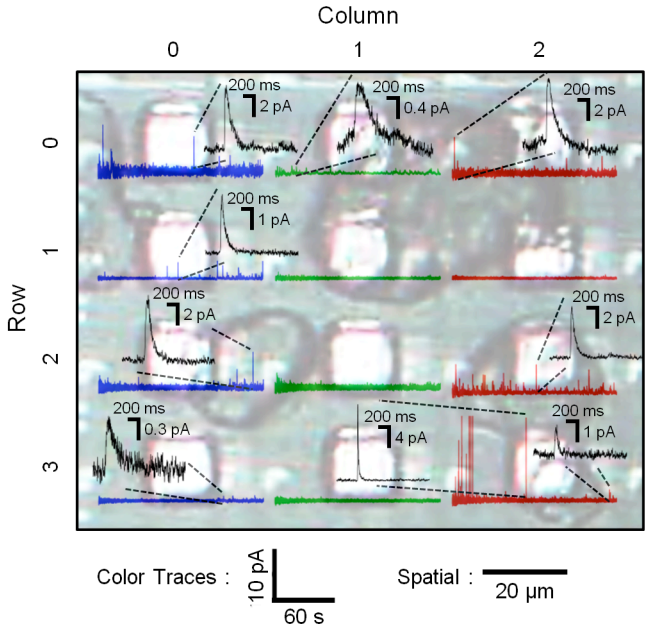

Figure 2.5. Live chromaffin cell recordings of neurotransmitter release. Chromaffin cells were cultured on-chip 24 hrs prior to the recording. Photograph showing 12 of 100 electrodes partly covered with cells atop. Cells were stimulated by 70 mM KCl. The amperometric traces from each electrode are superimposed. Black traces show individual events on expanded scale depending on individual amperometric spike amplitudes. The size of an individual cell (column 2, row 3) was typically < 20 µm. Aggregated cells that is > 20 µm were found on column 0 × row 1 ~ row 2, column 1 × row 0 ~ row 1, and column 2 × row 0 ~ row 2 electrodes.

The other electrodes with cell aggregates on them detected spikes that had half-width > 100 ms, which was presumably caused by the diffusional broadening that reflects the increased traveling distance before released molecules reached the electrode [15, 39]. Accordingly, electrodes (column 0 × row 0 and row 3) without direct contact to a cell recorded spikes that were very small and slow, presumably originated from release events of distant cells. This parallel recording of amperometric spikes confirmed the biosensor's capability to record quantal release events simultaneously from live-cells over the typical recording time (~ 150 seconds) with sub-millisecond resolution, pico-ampere current resolution, and stability without a

significant baseline drift over time that is comparable to conventional low-noise amplifiers. In some cases, such as the electrode in column 1 - row 1, no amperometric spikes were recorded although a cell appeared to be present over the electrode. The absence of amperometric spikes could simply be explained by inactivity of the cell. However, it should be noted that this electrode was covered by part of a cell aggregate such that the space between a chromaffin cell and the electrode may have been obstructed by other material preventing rapid diffusion of released molecules from the cell surface to the electrode.

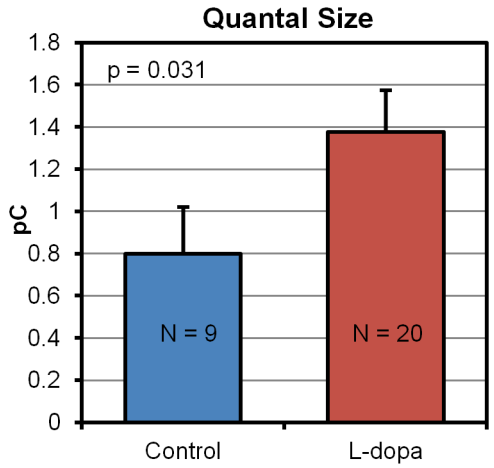

Figure 2.6. The effect of L-dopa on quantal size revealed by IC biosensor. The number of cells measured for control group and L-dopa treated group was 9 and 20, respectively. The mean quantal size was 73% larger by the effect of L-dopa compared to the control group. Student t-test value (p) for the group comparison was 0.031.

To demonstrate the detection of a change in quantal size, cells cultured on the chip were incubated with a solution containing 200 µM L-dopa for 1 hour before the experiment. To account for cell-to-cell variability the median of individual quantal size values was determined for each electrode that registered at least 3 events, giving an estimate of quantal size for each electrode [14], presumably dominated by release events from one cell. Subsequently, the mean of the median values was determined. The quantal size obtained in this way for L-dopa treated cells (1.38 pC) was significantly larger ($p<0.05$) than that obtained from control cells (0.80 pC) incubated on a different chip in the absence of L-dopa (Fig. 2.6). The recording took less than 20 minutes for both, the control and the L-dopa treated cells.

2.5. Discussion

Neurotransmitter release occurs in the form of quanta from vesicles that fuse with the cell membrane. The amount and time course of release can be recorded as an amperometric spike using microelectrodes Amperometric recordings revealed that quantal size is increased by the Parkinson's drug L-Dopa and decreased by reserpine [23, 31, 32]. Treatment with botulinum toxin A (Botox) reduces the rate of release events, and changes the properties of the fusion pore, without affecting quantal size [6, 33]. It is of great interest to develop a high-throughput technology to characterize the modulation of transmitter release by drugs or molecular manipulations.

The array presented here is optimized primarily for recording of single vesicle release events. By their nature, these events originate from vesicles ~200 nm in diameter and the released molecules produce a finite charge and current. The ideal electrode has therefore a size that is similar to the size of the cell to maximize the capture of release events from the cell surface. Our design incorporates such cell-sized microelectrodes. Larger electrodes produce increased noise [40] but not a larger signal and therefore reduced signal-to-noise ratio. For this reason recordings of single release events are generally performed with microelectrodes.

In recent years, planar microelectrode arrays have been fabricated for the measurement of quantal release using different materials to create polarizable electrodes suitable for amperometric recordings. These include platinum [41, 42], pyrolyzed photoresist [43], carbon [38, 44], ITO [10], nitrogen-doped diamond-like carbon (DLC:N) [45], boron-doped nanocrystalline diamond [46] and organic polymers [47]. The limitation of such microelectrode arrays is that for parallel recordings each electrode needs to be connected to an external amplifier, and such devices are therefore not scalable. Few attempts have been made to integrate polarizable electrochemical electrodes with a potentiostat array on-chip [48-50]. Only one of these devices allowed simultaneous measurement from multiple electrodes, but the synchronous integration and readout periods produced a minimum 3.2 ms dead time during readout of the array [50].

The time-division multiplexing we demonstrate here reduces the readout dead time by more than two orders of magnitude to 25 μs. Furthermore, the half-shared amplifier structure we use here [34] reduces the area of the repeating amplifier unit to 0.0009 mm^2, which approaches cellular dimensions and makes the technology truly scalable. To our knowledge, we demonstrate for the first time the simultaneous on-chip recording of quantal release events from living cells on a 100-electrode array.

Amperometric spike time course, amplitude and charge can be affected by the diffusion distance between the release site and the amperometric electrode as has been shown for carbon fiber microelectrodes [51]. Release events from an area of a cell that is not in direct contact with the electrode will produce smaller and slower amperometric spikes due to diffusion [15]. The results of Fig. 2.5 show that single release events with rapid amperometric spikes are successfully recorded when a single cell adheres to an electrode, whereas cell aggregates produce smaller and slower amperometric spikes, presumably reflecting hindered diffusion. This limitation may be overcome by incorporating features that improve targeting of individual cells to individual electrodes using chemical or mechanical cues as shown in [45, 52]. Cells located between electrodes could generate small and slow amperometric spikes at adjacent electrodes, if the adjacent electrode is not covered by another cell. Increasing spacing between electrodes would not necessarily help. Recording of amperometric spikes distorted by diffusional broadening will be minimized by improved electrode coverage by effective cell targeting.

The detection of a significant increase in quantal size following L-dopa treatment using the IC biosensor array demonstrates the successful application of the method described in this chapter for the identification of a drug manipulation. The increased quantal size by L-dopa agrees well with the previously reports on the effect of L-dopa [5]. The data collection only took less than 20 minutes for both groups, which is vastly accelerated compared to traditional methods which can only conduct recordings one cell at a time. It can be applied in the future to reveal the modulation of transmitter release by existing and newly developed drugs with high throughput.

In addition to the single cell measurements the scalable array presented here may be used to obtain spatial information of DA release in the brain. A recent publication [53] describes a linear microelectrode array comprising four carbon-fiber microelectrodes spaced 250 μm apart that revealed heterogeneous DA release in the striatum of anesthetized rats. While the device we describe here is not designed for fast scan cyclic voltammetry, such a modification will be possible. The ability to include hundred or even more electrodes on a chip with ~ 1 mm dimensions would provide enhanced spatial resolution for the characterization of the spatiotemporal dynamics of DA release.

Chromaffin cells release adrenaline or noradrenaline and the use of Pt electrodes with a potential of 700 mV ensures detection of both transmitters with equal efficiency. However, specific functionalization of individual electrodes for detection of other compounds, in particular pathogens that are not per se oxidizable, would be possible [54]. The main limitation of such biosensors is the generation of nonspecific currents by different electroactive compounds leading to potential interferences [55]. The array technology described here would allow inclusion of several differently functionalized electrodes together with a number of non-functionalized "control electrodes" to distinguish specific and non-specific responses.

2.6. Conclusions

In this work, we presented an electrochemical biosensor array with high throughput capability. It incorporated an array of low-noise CMOS potentiostats using a shared amplifier structure with very small footprint area [34]. We have shown here that conformal deposition of Pt, as a polarizable electrode material was a robust process allowing on-chip application of aqueous solutions and parallel measurements of oxidizable transmitters from 100 electrodes. The biosensor allowed on-chip cell culture of 3 days in the incubator preceding stimulation and amperometric recordings. The recordings had low stable baseline values for the recording time of up to 5 minutes. Time-resolved measurements of the

oxidation currents induced by DA injection demonstrate the ability of this amperometric detector array to record simultaneously with all 100 electrodes. The device shows dose response linearity and could spatially resolve the current traces indicating the diffusion path of the molecules. Results from live-cell amperometry demonstrated the functionality of this biosensor's application for analysis of quantal release events with a sensitivity of ~6,000 molecules. The pico-ampere current resolution and the effective time resolution of 500 μs are suitable to resolve single vesicle secretion events from chromaffin cells. The amperometric spike parameters recorded with this array were consistent with previous carbon fiber recordings [11, 12]. Finally, a significant increase in quantal size after incubation of cells with L-dopa was detected using the electrode array, fully consistent with previous reports [5], demonstrating the successful use of the IC biosensor for high throughput drug screening.

2.7. Notes to Chapter 2

The work described in chapter 2 was done with the contributions from other co-authors; Brian N. Kim designed the work and conducted the fabrication of IC biosensor and experiments as well as the analysis; Adam D. Herbst developed the demultiplexing software; Sung June Kim contributed on the design of IC and troubleshooting; Bradley A. Minch designed the half-shared amplifier; Manfred Lindau designed the work. The authors thank Joan S. Lenz for her flawless technical assistance during this research, Qinghua Fang for the culture of chromaffin cells, and Sunitha Ayers for comments on the manuscript. Post-fabrication was performed in Cornell Nanofabrication Facility (CNF) and Nanobiotechnology Center (NBTC) at Cornell University, Ithaca, NY. The IC design and simulations were done in Tanner Tools EDA software. Electrostatic discharge (ESD) protection pad design was taken from the Tanner Tools design library. This work was supported by National Institutes of Health (NIH) grants R01MH095046, and T32GM008267, and National Science Foundation Agreement No. DGE-0654112 (IGERT program)

administered by the Nanobiotechnology Center at Cornell University. This work has been published in Biosensors & Bioelectronics [56].

CHAPTER 3

TAPE-OFF: AN IMPROVED POST-FABRICATION FOR HIGH THROUGHPUT BIOSENSOR ARRAY WITH 320 ELECTRODES

3.1. Abstract

Sensing electrodes can be directly integrated on top of Integrated Circuit (IC) chips by post-processing the CMOS IC using microfabrication techniques. This process is known as post-fabrication and requires sophisticated handling because IC chips are fragile and can be easily damaged by commonly introduced. Here, we present a new patterning method called "Tape-off" instead of commonly used photolithography. Tape-off involves only few steps, significantly shorter than photolithography and does not require microfabrication equipment. It produces a self-aligned pattern, and thus avoids misalignments as many occur in photolithography. Post-fabricated biosensor array exhibited a stable performance with electrolyte contact and measured dopamine molecule oxidation successfully. The biosensor array was able to directly interface with living cells and measure neurotransmitter release from individual vesicle secretion. The tape-off method may enhance the efficiency of post fabrication for on-chip biosensor arrays as well as other applications.

3.2. Introduction

Post-fabrication refers to a fabrication applied to Integrated Circuit (IC) chips after IC fabrication from the semiconductor company. The Integration Circuit (IC) technology allows very-large-scale-integration (VLSI) of amplifying and other signal processing circuits in a small chip. Through post-fabrication, working or sensing electrodes can be built right on IC chips to create an active IC-based sensor or biosensor. Integration of signal processing circuits and sensing electrodes with sub-micrometer

interconnections in a single microchip device offers multiple advantages such as reduction in noise, high throughput, and portability [56].

However, despite of the advantages, such post-fabrication is difficult to use because the yield of post-fabrication is low and fabrication methods are limited due to IC chip's temperature and electrostatic sensitivity, and chemical reactivity of the IC surface. Post-fabrication is typically done using photolithography with a careful handling of IC dies. During post-fabrication of sensing electrodes on the IC surface, the electrode layer requires an alignment to vias (Vertical Interconnect Access, typically AlCu) to establish contacts to the underlying circuits. The alignment in die-based post-fabrication is inaccurate compared to wafer-based fabrications, because the photoresist layer spun on a die lacks surface uniformity that results in an imperfect contact between the mask and the die. In such cases, the misalignment is difficult to avoid. In a previous report when a 15 μm × 15 μm platinum electrode was patterned on an electrochemical biosensor array, 2-4 μm of misalignment was typical [56]. Here, we describe a new lift-off method, called tape-off, to selectively pattern metal (or desired materials) in vias without photolithography.

3.3. Results

In Fig. 3.1a, a schematic illustration of the surface of an IC die is shown. The interconnections (via) from the underlying circuits to the surface working electrodes are AlCu alloy and the passivation (Oxide) covering the AlCu surface is removed as a part of IC fabrication prior to post-fabrication. Platinum, a common material for post-fabrication of electrochemical sensors, is coated on the surface by e-beam physical vapor deposition (Fig. 3.1b). In the next step, the wafer-dicing tape is gently placed on top of the die as flat as possible, with the adhesive-side facing downward (Fig. 3.1c). The placement of tape is followed by press-rolling to tightly attach the tape to the surface and remove any air bubbles that may be trapped in between the tape and the IC surface (Fig. 3.1d). We used a press-roller with wafer/film frame

tape applicator. In Fig. 3.1e, the tape is removed by lifting it up from one side to the other. The metal layer that made physical contact with the tape is removed from the surface of IC by the strong adhesion created by the adhesive side of the tape. However, the metal layer inside the cavities of vias remain because the adhesive tape makes close contact to the surface during step c and d in Fig. 3.1, while the lower (or recessed) compartment of the cavity does not make a physical contact with the tape. Thus, the tape-off procedure will result in a self-aligned pattern of working electrodes (Fig. 3.1f).

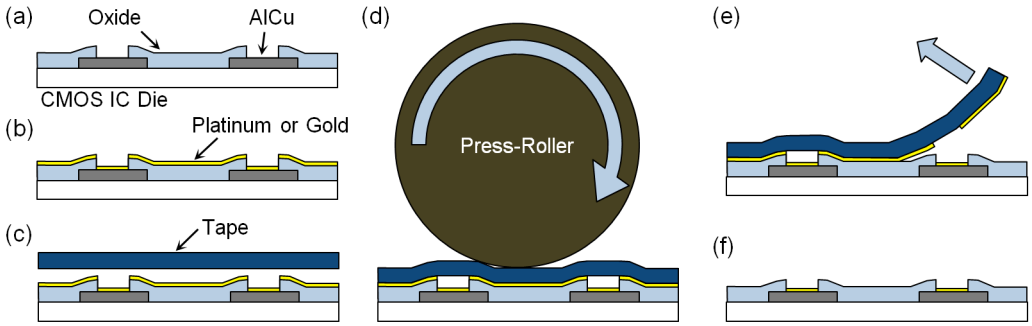

Figure 3.1. Post-fabrication using tape-off, (a) the surface of IC die, two micro-cavities with AlCu alloy via in the lower compartment is shown. The cavity is 1.5 µm deep and 10 µm wide. (b) thin film deposition of platinum or gold, (c) adhesion of tape on the metal-deposited die, (d) press-rolling of the surface to introduce a tight adhesion of metal and the tape, (e) the removal of the tape with metal, (f) patterned metal on lower compartment of the cavities that will serve as working electrodes in IC biosensor.

The result of the tape-off application to post-fabrication is shown in detail for a single electrode in Fig. 3.2. Using energy dispersive X-ray spectroscopy (EDX), the materials in and around the cavity at the via were examined. Spot A (in Fig. 3.2a) is located in the lower compartment (between lines labeled “2” in Fig. 3.2b) of the cavity and is originally AlCu before post-fabrication. The result of EDX revealed platinum on spot A instead of AlCu as shown in Fig. 3.2c. Spots B, C, and D (between lines labeled “1” and “2” and outside lines “1” in Fig. 3.2b) were originally silicon oxide or silicon nitride and remained the same after post-fabrication, while a Pt peak was not detectable. The EDX results clearly prove that the tape-off tape was able to selectively remove the Pt layer on the upper surfaces (on the oxides), leaving a Pt pattern inside the well on top of the AlCu via, without the need for any alignment process. Thus, tape-off produced a self-aligned pattern of metal.

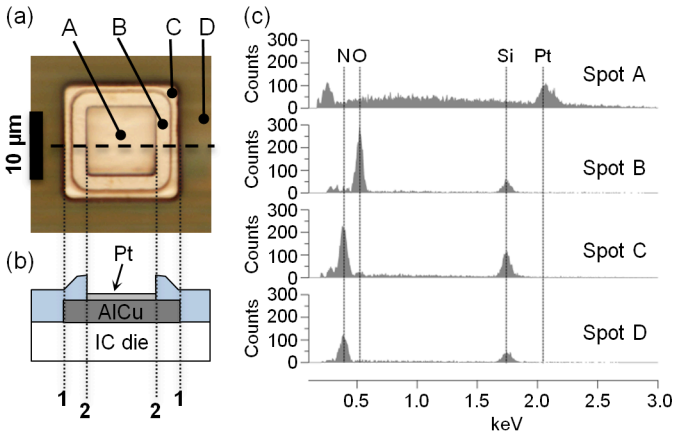

Figure 3.2. X-ray analysis of patterned surface after tape-off. (a) Microphotograph of a single working electrode on IC die after post-fabrication of platinum, (b) a cross-sectional view along the dashed line in panel a. (c) energy dispersive X-ray (EDX) spectrum of spots in panel a. Spot A is the lower compartment of the cavity created by the thick oxides and platinum is found dominantly. On spot B, C, and D where platinum was initially deposited and removed by tape-off, no platinum was detected and only silicon oxide or silicon nitride is found, both commonly used as oxide passivations in IC fabrication.

The tape-off post-fabrication method was validated by post-fabricating an electrochemical detection IC sensor and measuring oxidation of dopamine (DA), an electroactive neurotransmitter. Using IC technology, high-throughput electrochemical detectors including current-to-voltage amplifiers and time-division multiplexers were integrated into the IC die by the IC fabrication [56]. The amplifiers served as potentiostat to hold electrodes at constant 700 mV and measured biomolecules, in this case DA, oxidized at the electrode surface. Electrochemical detection requires the electrode material to be polarizable, for example, gold or platinum. For this application, platinum was deposited and wafer dicing tape was used for tape-off. Fig. 3.3a shows an array of 320 electrodes and underlying circuits after post-fabrication using platinum tape-off. An image of the tape that was used for taping-off platinum on this specific array is shown in Fig. 3.3b. It shows essentially a negative of the electrode array pattern with all the platinum removed from the surface of IC sensor residing at the adhesive side of tape, as evidence of successful lift-off of platinum. The dark squares (zoomed in photograph, Fig. 3.3b inset) is the region where the platinum was not taped-off and stayed at the surface of AlCu via (Fig. 3.3a inset). The platinum patterns produced by the tape-off process appeared accurate for all 320 electrodes without leaving any retention.

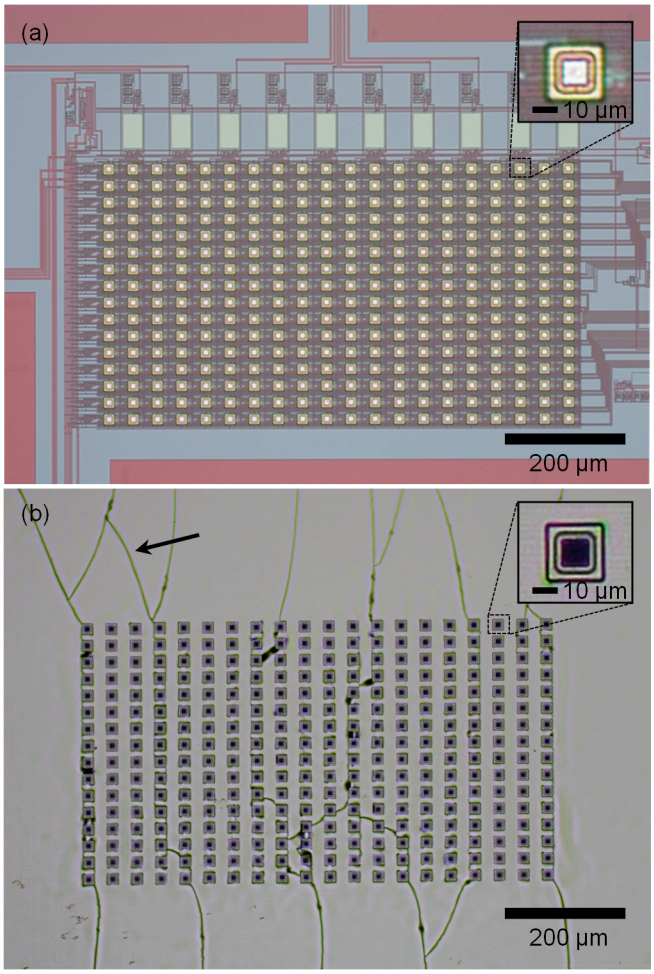

Figure 3.3. Photograph of resulted pattern on IC sensor and adhesive tape used for tape-off. (a) An electrochemical IC sensor array after tape-off of platinum. It consists of 320 surface electrodes and amplifiers. (b) Photograph of the tape on adhesive side after tape-off. Silver color is the platinum layer and black indicates the absence of platinum on the tape. Platinum layer removed from the surface of IC sensor resides on the tape. The absence of platinum at the center of each square is an indication of success pattern of platinum at the surface of AlCu via. The arrow indicates the crack on platinum which was caused the bending of tape during tape-off process.

The post-fabrication quality was further examined by measuring DA oxidation. The electrode array was initially covered with 50 µL of 150 mM NaCl electrolyte, which produced a very small baseline current level (preceding pink box 1 in Fig. 3.4a) by the electrode/electrolyte interface. The baseline current was on average −1.5 pA for all 320 electrodes (the blue bar in Fig. 3.4b), suggesting that the current through the electrode/electrolyte interface is negligibly small. The small baseline current, the oxidation current from molecules of interest can be distinctively identified.. During the time period indicated by pink box 1

in Fig. 3.4a, the DA solution (50 µL of 606 µM) was injected into the electrolyte covering the array, giving a final concentration of 303 µM in the total 100 µL solution. The electrolyte with DA was vigorously mixed by pipetting, during the time period indicated by pink box 2 in Fig. 3.4a, to equilibrate the DA concentration such that the variation of oxidation current measured by each electrode is minimized. The averaged current level at 35 sec for all 320 electrodes was 39.5 pA (Fig. 3.4b). The DA oxidation current is 41.0 pA, calculated by subtracting the baseline current.

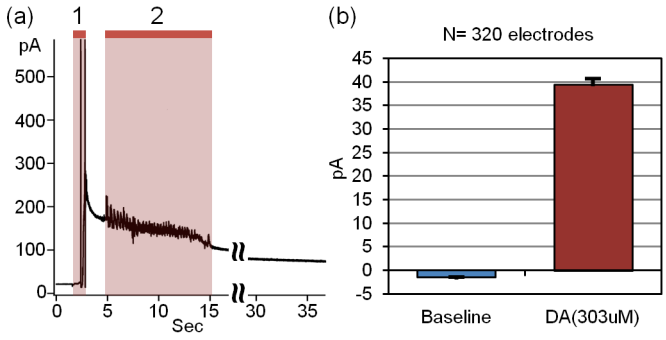

Figure 3.4. Current measurements of dopamine (DA) oxidation under electrolyte contact. (a) A recording of DA from an electrode among a 320 electrode array. The array is initially covered with 50 µL electrolyte, and 50 µL of 606 µM DA injected using a pipette during pink box 1. During pink box 2, vigorous pipetting is applied to reach a final concentration of 303 µM. After 30 sec, the current reached a steady-state current. (b) The average baseline current of all 320 electrodes prior to DA injection is −1.5 ± 0.1 pA. At the final concentration of 303 µM DA, the current is increased to 39.5 ± 1.3 pA. The error bar is in SEM.

To determine if the electrode array is stable in the presence of living cells, 10 µl of chromaffin cell suspension was added and the cells were given 5 minutes to settle and adhere to the electrodes. Neurotransmitter release from the living cells was stimulated by injection of high K^+, which produced amperometric spikes as shown in Fig. 3.5a for one selected electrode. On an expanded scale, a series of amperometric spikes is shown. These spikes exhibits the typical shape of amperometric spikes with a steep increase followed by a relatively slow decay. The mean values of half-width, I_{max}, and quantal size were 12.4 ms, 32.2 pA, and 0.50 pC, respectively. The spike parameters collected using the 320 electrode array are consistent with previous reports [11, 12].

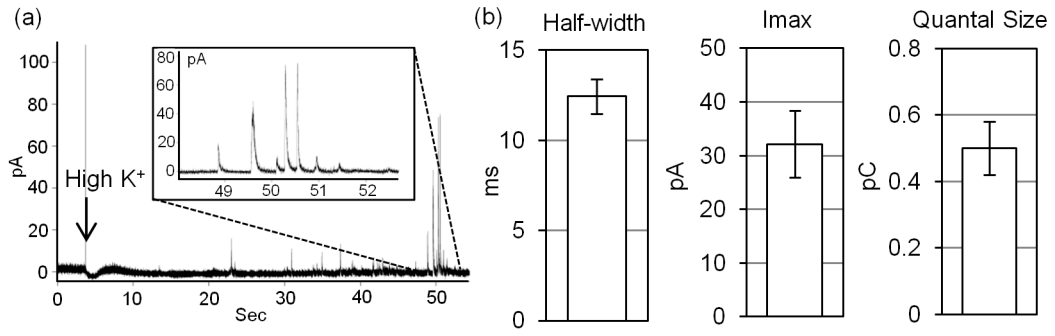

Figure 3.5. Live-cell measurement of the 320 electrode array post-processed by tape-off. (a) A current trace measured from one electrode. At the time indicated by the arrow, high K^+ was introduced to the cell for stimulation. Spikes represent each vesicle release. The expanded graph at near 50 sec shows measured spikes with the typical shape of amperometric spike. (b) Total of 11 cells were successfully measured and the mean spike parameters (half-width, I_{max}, and quantal size) are shown in bar graphs. The error bar is in SEM.

3.4. Conclusion and Discussion

We demonstrated an improved post-fabrication method named tape-off. Conventionally used post-fabrication methods are based on photolithography. In order to pattern and align electrodes on the IC, photoresist is patterned to transfer the image pattern to the deposited metal by lift-off or etching. Unlike previous post-fabrication methods that rely heavily on photolithography, tape-off doesn't require photoresist and thus the lack of photoresist uniformity is irrelevant. The application of tape-off to post-fabrication is a quick and is an alignment-free process. Tape-off is an ideal post-fabrication method for a die-based process avoids many of the disadvantages and difficulties of photolithography-based post-fabrication such as frequent misalignments, possible damages to AlCu by the chemicals used during photolithography, and low reproducibility. EDX and microscopic inspection revealed an accurate pattern of the metal into the cavity that is originally created by IC fabrication from the semiconductor company. The process was validated by creating an electrochemical detection IC sensor and electrochemically recording DA oxidation. The baseline current measured was negligibly small which reflects a very high electrode/electrolyte interface resistance and, thus, the good quality of Pt layer. It successfully measured

the oxidation of DA, proving the successful implementation of tape-off to the field of IC biosensor. The electrode array was able to detect neurotransmitter release from chromaffin cells. The mean spike parameters, half-width, I_{max}, and quantal size, measured by the tape-off processed biosensor were consistent with previous results from CFE recordings [11, 12].

The tape-off technique can be used to pattern metal, but also any type of molecules and biomolecules including protein and polymer brushes such as polylysine, typically used to enhance cell adhesion. Because tape-off is a completely dry process unlike photolithography that introduces contacts to chemicals, such as photoresist, developer, and photoresist remover, tape-off may also be useful in the patterning of biological substances and organic materials. This is similar to micro-contact printing [57] and the parylene peel-off [37] that limits the contact of the target material to photolithography solutions. The parylene peel-off works by pre-patterning parylene film using photolithography. This is followed by deposition of the target material on the parylene film. By peeling off the parylene film, the target material sitting on top of parylene is removed. As a result, a negative image of parylene pattern is transferred to the target material layer. One advantage of tape-off compared to parylene peel-off or other biocompatible processes is that parylene peel-off (and most other processes) is not self-aligning but relies on photolithography mask alignment to pattern parylene (or other image-transferring media). Thus, it cannot be repeated unless the parylene film (or other image-transferring media) is re-patterned or re-aligned which require a series of photolithography steps that may take over 6 hours using expensive equipment, including parylene coater, photoresist spinner, aligner, and plasma etcher. Tape-off can be easily repeated in few minutes to result in a self-aligned pattern, once the permanent cavities have been defined and require a minimum or no equipment. The rate of success of tape-off depends on the topology of cavities especially the aspect ratio (depth/width). When using large AlCu vias with a width above 100 µm and the depth of 1.5 µm, the Pt layer covering AlCu vias was often removed or damaged after tape-off. But with a higher aspect ratio (10 µm width and 1.5 µm depth), a success rate of 100% was achieved. This is because

the tape is more likely to establish physical contacts during tape-off with the recessed surface of cavities when the aspect ratio is low.

3.5. Material and methods

Platinum was deposited at 0.1 nm/s using CHA 50 e-beam evaporator. Wafer-dicing tape was used for tape-off on the IC and the press-roller attached to Semiconductor Equipment Corporation's model 3100 wafer/film frame tape applicator was used for press-rolling.

The standard solution contained 140 mM NaCl, 5 mM KCl, 1 mM $MgCl_2$, 10 mM $CaCl_2$, and 10 mM HEPES/NaOH (pH 7.3) with the osmolality adjusted to 300 mmol/kg by adding glucose. The high K^+ stimulating solution contained 140 mM KCl, 5 mM NaCl, 1 mM $MgCl_2$, 10 mM $CaCl_2$, and 10 mM HEPES/NaOH (pH 7.3) with the osmolality adjusted to 300 mmol/kg by adding glucose. For DA measurement, the electrode array was covered with 50 µL of standard solution and DA was injected using a pipette adding 50 µL of standard solution containing DA at the concentration of 606 µM.

Bovine adrenal glands was cultured as described [35]. Cells were suspended in the standard solution and 10 µL of suspended cells were placed on the Poly-D-Lycine (0.05%) coated biosensor for 5 minutes which was followed by the recording. For the cell stimulation, 10 µL of high K^+ solution was added to the standard solution, resulting in a final concentration of 70 mM of KCl.

3.6. Note to Chapter 3

The work presented in Chapter 3 is filed for a US patent application titled, "Dry and self-aligned lift-off method". The U.S. Patent Application number is No. 61/732,982.

CHAPTER 4

PORTABLE DATA ACQUISITION SYSTEM FOR HIGH THROUGHPUT RECORDINGS

4.1. Introduction

High throughput recordings with large sensor arrays and sub-miilisecond time resolution generates very large amounts of data that needs to be acquired and stored in a computer system. We developed a portable and low cost data acquisition system incorporating ten analog-to-digital converters (ADCs) to sample simultaneously ten channels of analog data with 12-bit resolution and 20 kS/s sampling rate, generating a total data rate of 200 kS/s. The board was designed to operate a 10 x 10 CMOS potentiostat array with on-chip working electrodes for amperometric sensing. For each 10-electrode column, the potentiostat array presents data at a single analog output by time division multiplexing such that the 10 ADCs sample the outputs of all 100 electrodes. The digital data was transferred through a single universal serial bus (USB) port to a computer. The data acquisition system was assembled on a single 3" x 4" board that was powered through the USB port, making the system easily portable. The recording software performs de-multiplexing of the data and displays the data from one selected electrode in real time during data acquisition. The functionality of the data acquisition system was validated by measuring oxidation of dopamine ejected onto the surface of the electrochemical detector array.

4.2. Results

The printed circuit board (PCB) for the data acquisition system consists of the following functional blocks (Fig. 4.1a): Replaceable IC biosensor array, bias circuit, clock generator, 12-bit ADCs, and USB transceiver. The replaceable IC biosensor array incorporates 100 electrochemical microelectrodes

connected to 100 integrating potentiostats with parallel recording capability from all 100 electrodes [56]. Through time division multiplexing, analog samples from 10 electrodes are presented serially at a single output pin (10-to-1 multiplexing). The sensor chip has 10 outputs to simultaneously record from all 100 electrodes. Operations of electrochemical recordings and 10-to-1 multiplexing were performed in the IC chip. Bias circuits and clock generator are components of the data acquisition board that provide control over the sampling rate, gain of I-to-V amplifier, output offset, and electrode voltage of the IC sensor array (Fig. 4.1b). To operate the ADCs, the clock generator produced clock pulses that were synchronized with the clocks for IC biosensor. The sampling by the ADCs is thus completely synchronous with the presentation of the analog data at the ADC inputs minimizing the number of samples required to acquire all the data the IC biosensor is streaming out. Thus, one digital value was transmitted for each potentiostat output sample optimizing the USB data transmission efficiency. Typically, each electrode was sampled at 2 kSample/s (kS/s), defined by the clock generator. Through time-division multiplexing of 10 electrodes in the IC, one output of IC biosensor presents 20 kElectrodeData/s of data and was digitized by an ADC with 20 kS/s rate,. One ADC therefore generates a serial data stream of 12 bits after each conversion/read phase. All 10 outputs from the biosensor presenting data from 100 electrodes were digitized with 10 parallel ADCs. ADCs were paired into 5 pairs and an additional 2-to-1 multiplexing was performed, fitting two ADCs into one digital output (40 kElectrodeData/s). Finally, all the multiplexed ADC outputs ($5 \times 40 = 200$ kElectrodeData/s; 100 electrodes with 2 kS/s each) were connected to a USB microcontroller for data transfer.

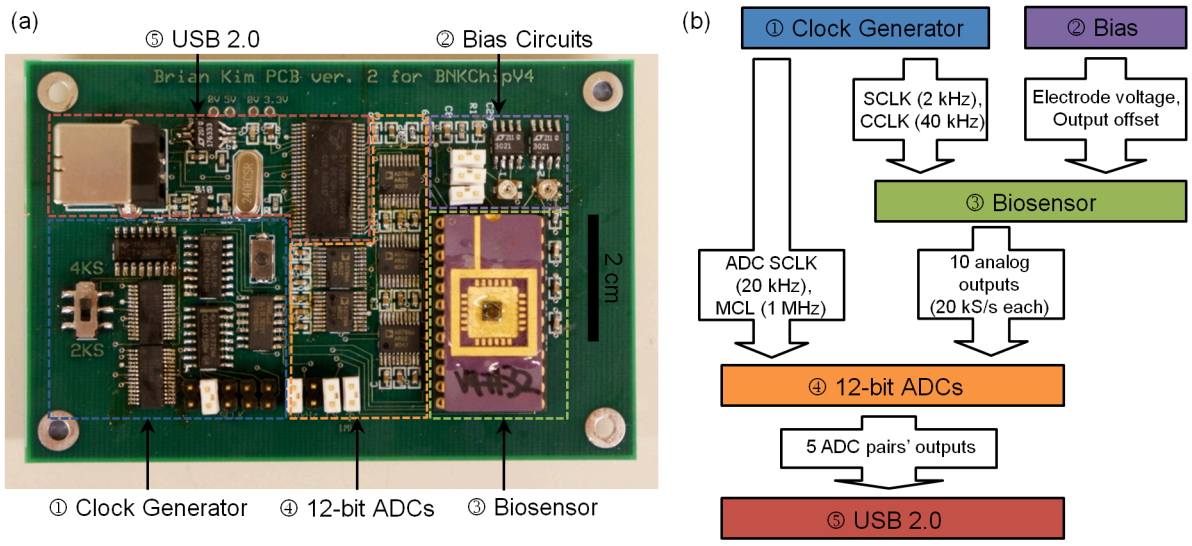

Figure 4.1. USB-communicating ADCs and the functioning blocks on PCB. (a) The PCB mainly consists of clock generator, bias circuits, biosensor, ADCs, and USB 2.0. (b) Functional relationships between the blocks in panel a. The clock generator and the bias circuit operate the biosensor and the output of the biosensor is sampled with synchronized ADCs. Finally the ADC data is sent through USB.

Digital data streams including outputs from 5 pairs of ADCs, 1 master clock (1 MHz) of ADC, 1 sampling clock (20 kHz) for ADC, and signal clock (2 kHz) for IC biosensor were efficiently multiplexed and sent simultaneously without any data loss or time delay through the USB port. This was accomplished by assigning each microcontroller (MCU) bit to a data stream and having all 8 MCU bits sent as a packet. Clock data sent through USB, excluding data from ADCs, were used as indicators during data demultiplexing to identify the time duration (width) of each ADC bit, indicating when ADCs' serial data stream starts and ends, and to which electrode the ADC data corresponds.

The communication to Cy7C68013A USB MCU from the local computer was supported by the driver produced by Saleae LLC. The driver included basic commands including a boot sequence to initiate MCU, start and end triggers for the packet streaming, emptying memory in MCU during data acquisition, and saving data into a binary file in the computer. The software for the user interface was incorporated in Igor Pro 6 (WaveMetrics). Because Saleae drivers work on C++ platform and Igor cannot directly

communicate through C++, an external operation (XOP) was created using the IGOR XOP toolkit (WaveMetrics) and Saleae drivers were incorporated in the XOP. As a result, procedures and functions in Igor were able to control the MCU through the XOP.

The user interface consists of 3 main panels: control panel, online display, and status display. In the control panel, basic settings such as the USB sampling rate and electrode selection for online display were provided. The optimal sampling rate was 2 – 4 MHz which is fast enough to sample the fastest clock (1 MHz, master clock for ADC) and is low enough that emptying data from computer RAM was faster than the rate of data streaming in. With the effective management of RAM, the recording was able to run without interruption until the hard drive was filled. Assuming that 2 MHz of USB sampling rate was used and 10 GB of hard drive space was available, the acquisition can run more than one hour long, which is sufficient because the electrochemical recordings in this application are typically no longer than 6 minutes.

The control of the data acquisition software is performed with only two buttons for start and stop of data acquisition. When the start for data acquisition is executed, the software initially checks for connection automatically and if MCU is operating normally, data streaming begins. In case when the USB connections are not established, the software establishes the USB connection and then initiate data streaming. To effectively use memory and reduce duplicating data in RAM, the USB data is immediately written to hard drive from XOP in binary format and the allocated memory emptied, instead of transferring data to Igor Pro 6. For online display of an electrode, stored data was loaded into the software as often as possible, and data older than 10 sec was erased from the RAM. Because screening through the entire data that was loaded for data display is inefficient and slow, the data from one specified electrode was selectively read for real-time online display. This was accomplished by introducing an initial period of phase identification, just before the actual recording started. In this initial period, the master and sampling clock of the ADC and the signal clock of the biosensor was carefully examined to determine the period (T) of a specific electrode output and the phase difference (ϕ) compared to signal clock. With known period and phase, the software reads the specific data set (serial 12 bits from a specific ADC)

within newly loaded data without de-multiplexing, which could take very long time because of multiple stages of multiplexing involved. In our testing environment (Desktop, i7 CPU and 4 GB RAM available to Igor Pro and SATA revision 3 with 6.0 Gb/s), the fastest frequency of the entire operation from data loading, demultiplexing, and display was 7 Hz. This allowed generation of a smooth online display. In a mobile setting (MacBook Air 2011), the frequency was slightly lowered to 5 Hz, which was still sufficient to generate a smooth online display.

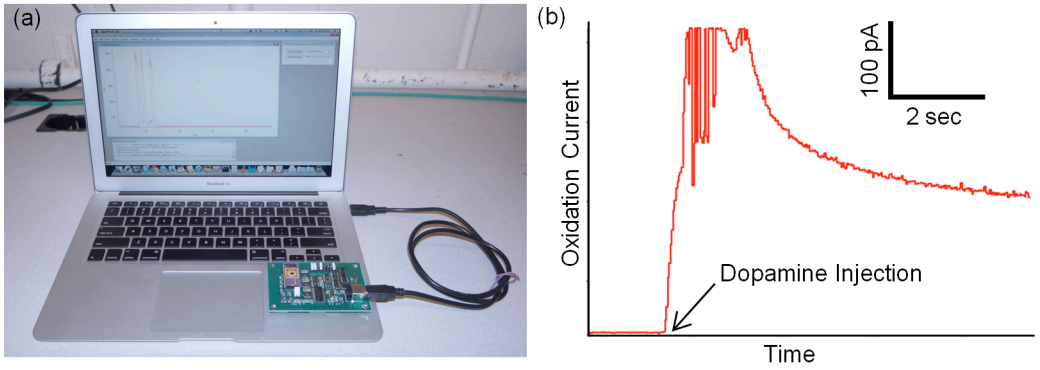

Figure 4.2. The portable recording setup using USB-ADC and the dopamine recording. (a) A MacBook Air 2011 model is operating USB-ADC connected through a USB cable. (b) The dopamine oxidation current measured by the IC biosensor and USB-ADC. After dopamine injection, the current steeply increased as the dopamine molecules hitting the electrode surface transfer electrons into the electrode.

In Fig. 4.2a, a portable recording setup using the USB-ADC is shown. No additional parts are required for the operation of electrochemical recordings because the USB-ADC is fully powered and operated by the laptop. The performance of the data acquisition system with the IC biosensor was evaluated by measuring the dopamine (DA) oxidation. The IC biosensor was initially covered with 50 µL of 150 mM NaCl solution and later injected with 50 µL of 685 µM DA and 150 mM NaCl solution. The analog data measuring the DA oxidation current from the IC biosensor was sampled by the ADCs, transmitted via the USB port and stored in the laptop. In Fig. 4.2b, the de-multiplexed data for one electrode is shown. After DA injection, a steep increase of current is evident, indicating the increasing concentration of DA at the surface of the electrode. The solution covering the IC biosensor was vigorously mixed using pipette

(reflected as spiking noise in the current trace) to assist the equilibration of the DA concentration. The current decayed as the final DA concentration was established through the DA diffusion.

	USB-ADC (In this Chapter)	Low-cost PCI-ADC	Low-cost USB-ADC
Description	Custom-made USB	PCI-6010 from NI	USB-6008 from NI
Portability (Laptop Compatible)	Yes (154 cm^3)	No (Require Desktop)	Yes (161 cm^3)
# of SE Channel	10	16	8
SE ADC bits	12-bits	16-bits	11-bits
Total Sampling Rate	400 kS/s	200 kS/s	10 kS/s
Input Range	0 – 5 V	± 5V	± 10
Cost	130 USD	484 USD	204 USD

Figure 4.3. The comparison of specifications and cost of different USB-ADCs. The most outperforming specifications among three ADCs are colored green, and among two USB-ADCs are colored yellow. The USB-ADC presented in this chapter outperformed the other ADCs although the cost is the lowest. The costs for PCI-6010 and USB-6008 were obtained from NI.com.

In Fig. 4.3, the cost and performance comparisons between the USB-ADC system presented here and some commercially available ADCs are shown. Because the emphasis of the work in this chapter is low-cost, ADCs with lowest costs were selected from National Instrument (NI). The most outperforming features are color coded green and the superior specification from two USB-ADCs are color coded yellow. Because PCI (Peripheral Component Interconnect) bus is natively faster than USB bus, PCI-ADC outperformed the other ADCs in the number of channels and ADC bits. Despite of bus disadvantage, the USB-ADC demonstrated in this chapter was superior in total sampling rate by a factor of two. The total sampling rate of custom-made USB-ADC was tested up to 400 kS/s for reliable performance, but is able to operate with faster sampling rate by trading-off the total time of recordings. The system described in this chapter is lower cost compared to commercially available USB-ADC systems and outperformed in every specification except the input range. However, the input range can be simply broadened to ± 10V

by adding an attenuator at the input-end, but native range of 0 – 5V was maintained because it was sufficient for the IC biosensor application and offered a better bit resolution.

4.3. Material and methods

PCB was designed in expressPCB software and used the 4-layer option to compact the circuit and make it portable. The PCB design was submitted to expressPCB for manufacture. The components incorporated in the PCB were surface mounts and the key components are listed: cypress Cy7C68013A-56 for USB MCU, AD7866 for 12-bit ADCs, 24LC00 for 128-bit EEPROM, and ICS674R for frequency divider. The components were soldered manually in the lab.

Igor Pro version 6.22A, WaveMetrics, was used for software engineering platform. Saleae logic driver downloaded from Saleae LLC as a development purpose. Microsoft Visual Studio C++ Express, Microsoft Co., was used with Igor XOP Toolkit to develop USB driver. The development environment was Dell OptiPlex 990 with i7-2600 (3.4 GHz) CPU, 16 GB RAM, and SATA revision 3. It was tested on a portable computer, which was MacBook Air 2011 13-inch with i5 (1.7 GHz) CPU, 4 GB RAM, and SATA revision 2.

4.4. Conclusion and discussion

In this chapter, a very simple but powerful data acquisitions system incorporating ADCs and USB data transfer was described. The manufacturing cost was lower than the cheapest ADCs commercially available from National Instrument. Considering that fact that the USB-ADC shown in this chapter was produced in minimum quantity, the pricing can be even lower with large quantity manufacturing. With the lowest cost, it still outperformed in sampling rate and the portability compared to other ADCs. The

work in the chapter demonstrated the concept of simplifying and lowering the cost and added portability. With the USB-ADC and IC biosensor presented, the electrochemical recording is as simple as plugging in an USB connector and pressing a start button. The method to produce USB-ADC is not limited to amperometric recordings only but simply be customized to produce general-purposed ADCs and serve as a portable ADC device for variety recording applications.

CHAPTER 5

CONDUCTING POLYMER MICROELECTRODES TO DIRECTLY MEASURE NEUROTRANSMITTER RELEASE FROM SINGLE LIVING CELLS

5.1. Abstract

The efficient interfacing of electronic devices with living cells represents a key goal of bioelectronics. The use of organic electronic materials at this interface is currently receiving considerable attention due to the natural compatibility of organics with biological materials. Here we report a conducting polymer microelectrode capable of detecting transmitter release from single living cells. Using photolithography we fabricated microelectrodes based on poly(3,4-ethylenedioxythiophene) doped with poly(styrene sulfonate) (PEDOT:PSS), which are able to record the oxidation of catecholamines released from chromaffin cells during exocytosis with a high signal-to-noise ratio. This result represents a new capability for organic electronics that could lead to devices that interface in novel ways with the nervous system.

5.2. Introduction

Many cell types in the human body release specific transmitter molecules that are recognized by specific receptors in the target cell membrane. In a variety of excitable cells, such as neurons and neuroendocrine cells, the transmitter molecules are stored in membrane-bound vesicles. In response to stimulation, these vesicles fuse with the cell's plasma membrane, thereby releasing their contents in the form of quantal events [58]. This mechanism of vesicle fusion with the plasma membrane has been termed exocytosis. Chromaffin cells are a widely used model system to study neuronal exocytosis. These cells release the

catecholamines adrenaline and noradrenaline, which can be detected electrochemically using carbon fiber or microfabricated electrodes [59]. In order to investigate the exocytotic process of a single vesicle, the microelectrode held at ~700 mV is placed close to the cell surface and the exocytotic events are recorded by monitoring an electrical current. The latter results from the transfer of electrons that is associated with the oxidation of the released catecholamine molecules at the surface of the microelectrode. The resulting oxidation current reveals amperometric spikes that provide information about the frequency of release events, the number of released transmitter molecules from a single vesicle (quantal size) and the kinetics of quantal release events [11]. It also reveals the formation of an initially narrow fusion pore that manifests itself as a pre-spike feature, also called a 'foot' signal [12, 13]. While carbon fiber microelectrodes (CFEs) are used most widely, microfabricated planar electrodes made of platinum (Pt) [37, 41] or indium tin oxide (ITO) [60, 61] are being developed as a more convenient way to interface with cells. Large arrays of such electrodes can be easily fabricated, paving the way for massively parallel recording from networks of neurons. Moreover, by combining measurements using microfabricated electrode arrays with fluorescence microscopy imaging, the fusion of vesicles can be better understood [15, 62].

The advent of organic electronics has made available a host of materials and devices with unique properties for interfacing with biology [63, 64]. One example is conducting polymer electrodes that interface electrically with neurons, providing stimulation and recording of action potentials [65]. A second example is organic electronic ion pumps, that have been used to precisely deliver neurotransmitters to the appropriate neurons and control hearing in a mammal [66, 67]. These devices utilize conducting polymers such as poly(3,4-ethylenedioxythiophene) doped with poly(styrene sulfonate) (PEDOT:PSS), a material that has been shown to be biocompatible with a variety of different cells [63]. The "soft" nature of organics offers better mechanical compatibility with tissue than traditional electronic materials, while their natural compatibility with mechanically flexible substrates paves the way for the development of implants that better conform to the non-planar shape of organs. In this paper we

demonstrate that PEDOT:PSS can be applied for the direct detection of transmitter release from living cells, therefore enabling a chemo-electrical way to interface with the nervous system. This work paves the way for the design of artificial synapses, in which the capability of conducting polymers to deliver neurotransmitters for cell stimulation or inhibition can be combined with their ability to detect the release of neurotransmitters.

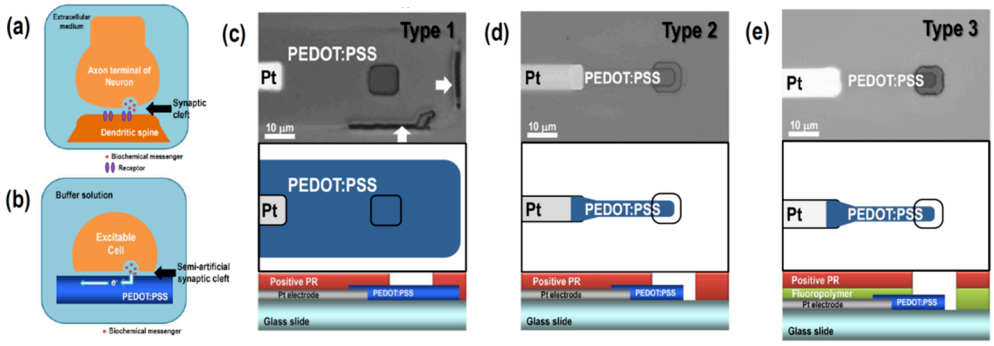

Figure 5.1. Cell interfacing PEDOT:PSS microelectrode and architectures. Analogy between a synaptic cleft in neurons (a) and a semi-artificial cleft at a cell/PEDOT:PSS interface (b). Optical micrograph (upper panel) and schematic top- and side-view (lower panel) of different architectures of PEDOT:PSS microelectrodes; (c) large size PEDOT:PSS island insulated with a positive-tone photoresist (device of type 1), (d) small size of PEDOT:PSS island insulated with a positive-tone photoresist (device of type 2), and (e) small size PEDOT:PSS island insulated using a fluoropolymer/positive-tone photoresist (device of type 3). The window on the insulator was 10 x 10 μm^2 in all devices, defining electrode areas of 100 μm^2 in device of type 1, 40 μm^2 in devices of type 2, and 30 μm^2 in devices of type 3. The arrows in panel (c) show the damaged part of the insulator.

5.3. Material and methods

5.3.1. Fabrication of PEDOT:PSS microelectrodes

In a synapse formed between an axonal nerve terminal of a pre-synaptic neuron and a dendritic spine of a post-synaptic neuron, the receptors in the post-synaptic membrane transduce the chemical signal into an electrical signal (Fig. 5.1a) Similarly, an excitable cell/PEDOT:PSS interface creates a semi-artificial synaptic cleft where the secreted transmitter molecules released by the cell diffuse to the PEDOT:PSS microelectrode surface and they are detected by producing an electrical signal (Fig. 5.1b). In an effort to

improve the quality of signal transduction, we progressed through three different device architectures, shown in Fig. 5.1c, d and e.

Pt microelectrodes (active area of 100 μm2) were fabricated by adapting a recipe reported in literature [41]. For the fabrication of the PEDOT:PSS microelectrodes, 15 nm thick Pt leads were defined on a glass substrate by conventional photolithography and electron-beam evaporation. A 5 nm thick titanium film was used as the adhesion layer. The PEDOT:PSS microelectrodes were subsequently fabricated by means of subtractive patterning: First, a PEDOT:PSS (Clevios PH500, HC Starck) solution which was formulated with ethylene glycol (EG, PEDOT:PSS/EG = 80/20 by volume percent) was spin-coated on the glass substrate with the Pt leads, and then dried at 140 Cº for 60 min. A protective layer that consisted of a fluorinated polymer (see inset of Fig. 5.2e) was then spin-coated on the PEDOT:PSS film from a ~ 9.1 wt% solution in 3M Novec Engineered Fluid HFE-7600, and baked at 110C for 10 min. On top of this fluorinated polymer film, photolithography was carried out using a AZ nLOF 2020 photoresist. PEDOT:PSS was patterned by etching the region where PEDOT:PSS was not covered by resist with oxygen plasma. The fluorinated polymer/photoresist layers were then removed by lift-off in 3M Novec Engineered Fluid HFE-7200.

The substrates were subsequently insulated, leaving only a small window open that defined the area of the microelectrode. For devices of type 3, a fluorinated polymer film (same as used above) was deposited on the substrates and was subsequently coated with Shipley 1805 (S1805) photoresist. The latter was exposed to UV in a contact aligner (ABM) to define a window over which the photoresist was removed to expose the PEDOT:PSS microelectrode. Development with aqueous alkaline developer (Shipley 300MIF) did not dissolve the underlying fluorinated polymer film, but did only the UV exposed areas of S1805 resist. The pattern in the S1805 resist was then transferred to the underlying fluorinated polymer layer by spin-coating HFE-7200 solvent for 10 seconds. Therefore, the final structure of the insulator consisted of a bilayer of the fluorinated polymer (~ 460 nm thick) and the S1805 layer (500 nm thick). The fabrication of devices of type 1 and 2 followed the same steps, but without the fluorinated polymer interlayer.

The difference between the three devices lies in the area of the PEDOT:PSS film and in the type of insulator: Devices of type 1 and 2 had the same insulator (a commercially available photoresist), but differed in the architecture of the PEDOT:PSS film, which had a smaller area in the device of type 2. As a result, the microelectrode area was 100 μm^2 in the device of type 1, and 40 μm^2 in the device of type 2. The device of type 3 utilized a geometry similar to device type 2 but had a slightly smaller PEDOT:PSS film area (the microelectrode area was 30 μm^2), as well as a bilayer insulator that included a fluoropolymer (insert of Fig. 5.2e shows its chemical structure) between PEDOT:PSS and the photoresist.

5.3.2. Cell preparation, electrochemical recording and analysis

Bovine adrenal glands were obtained from a local slaughter house and chromaffin cells were cultured on 8 mm cover slips as described in literature [35]. A cover slip with cultured cells was placed near the PEDOT:PSS microelectrodes, and a drop of buffer solution (~200 µl) was applied to cover the area including the microelectrodes and the cover slip with the cells. The buffer solution was composed of 140 mM NaCl, 5 mM KCl, 5 mM $CaCl_2$, 2 mM $MgCl_2$, 10 mM HEPES-NaOH and 10 mM D-glucose (pH 7.4). A healthy cell (shiny and roundish) was picked up from cover slip by applying gentle suction (~50 mBar) with a glass micropipette and was carefully moved and placed on a PEDOT:PSS microelectrode. The glass micropipette was also used to mechanically stimulate the exocytotic process by gently pressing on the cell.

The amperometric current was measured by single channel current amplifier (HEKA EPC-8, HEKA Instruments Inc.). The microelectrode was held at 700 mV relative to a Ag|AgCl reference electrode immersed in the buffer solution. The sampling rate for data acquisition was 2 kHz under the application of 500 Hz low-pass filter. Amperometric signals were further digitally filtered with a 500 Hz low pass Gaussian filter to reduce the background noise. Parameters obtained from amperometric spikes such as spike width at half maximum and amperometric charge were analyzed using Mosharov's Quanta Analysis

software (open source program available online, version 8.0) [36]. For a consistent comparison of analyzed parameter among different microelectrodes, standard deviations of noise (SD_I) for PEDOT:PSS microelectrodes were averaged and the cutoff peak height during analysis was set as four times of averaged SD_I (~12.84 pA).

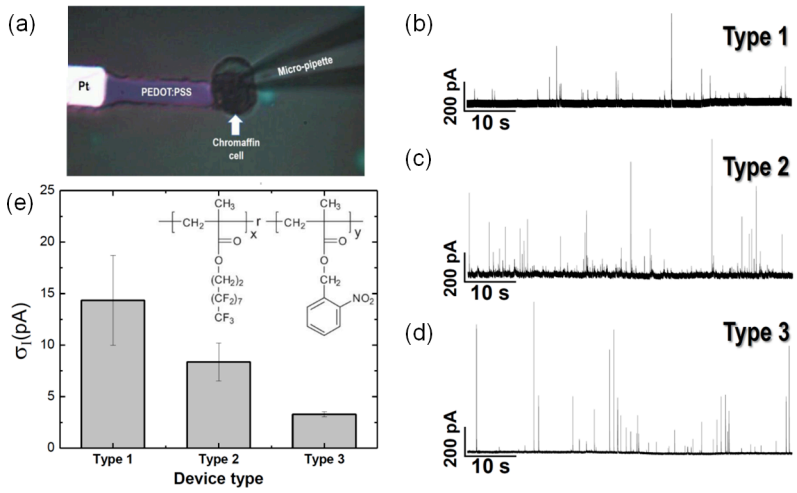

Figure 5.2. Amperometric recording of living cells using PEDOT:PSS electrodes. (a) Optical micrograph of the test configuration with single chromaffin cell placed on a PEDOT:PSS microelectrode of type 3. Current recording traces from devices of type 1 (b), 2 (c) and 3 (d). The spikes correspond to individual exocytosis events. Recordings were carried out by applying 700 mV to the microelectrodes, at a sampling rate of 2 kHz and through a 500 Hz low pass filter. (e) Quantification of electrode current noise for the three PEDOT:PSS microelectrode architectures. Current noises of seven microelectrodes were averaged for devices of type 1 and 3, and six microelectrodes were used for devices of type 2. The mean electrode current noise of type 1, 2 and 3 were 14.34±4.37 (N=7), 8.37±1.84 (N=6) and 3.29±0.24 pA (N=7), respectively. The error bars indicate the standard deviation. The inset in (e) displays the chemical structure of the fluoropolymer.

5.4. Results

Fig. 5.2a shows an optical micrograph of the test configuration of a device of type 3 with a chromaffin cell placed on top of the PEDOT:PSS microelectrode to monitor exocytotic events. By gently pressing on the cell with a micropipette for stimulation [15], amperometric spikes representing the oxidation of catecholamines released from individual vesicles were recorded with the PEDOT:PSS microelectrodes, as

shown in Fig. 5.2b, c and d. The applied potential was 700 mV relative to a Ag|AgCl reference electrode, which is comparable to values used with CFEs [11, 13, 51, 68] and Pt microelectrodes [15, 37, 41]. These results indicate that PEDOT:PSS microelectrodes have the ability to detect the release of transmitter molecules such as catecholamines.

The device architecture has a significant influence on the background electrode current noise during the measurement, as shown in Fig. 5.2e. Electrode current noise is, in general, proportional to the square root of the electrode area. Therefore, devices of type 3 which have the smallest PEDOT:PSS films are expected to show the lowest noise. Fabrication issues also play a role in determining electrode current noise: Patterning of the insulator layer of devices of type 1 and 2 (a positive-tone photoresist) to expose the PEDOT:PSS microelectrode surface necessitates a basic developer solution with a high pH (~14). It is known that the surface of PEDOT:PSS thin films consists of an excess PSS layer with acidic properties [69]. We find that the ensuing acid-base reaction that takes place at the surface of the PEDOT:PSS film causes a poor quality interface with the overlying photoresist layer. This effect can deteriorate the final pattern and lead to defects in the insulation of the PEDOT:PSS film, as indicated by white arrows in the micrograph of a device of type 1 in Fig. 5.1c. As a result, the rms electrode current noise was on average ~15 pA and showed considerable variability as indicated by the high standard deviation in Fig. 5.2e. Decreasing the size of the PEDOT:PSS film in devices of type 2 helped reduce the noise level (Fig. 5.2c and e). A further substantial reduction was achieved when a fluoropolymer interlayer was introduced between it and the photoresist layer in devices of type 3, as seen in Fig. 5.1d and e. The reduction by 61% in electrode current noise is much larger than that expected from the decrease in electrode area, which would be only ~13% when device of type 2 is compared with that of type 3. The success of the fluoropolymer lies in the fact that it can be processed from fluoroethers – solvents that are orthogonal to, hence do not affect the properties of most organic electronic materials [70]. Therefore, the use of a fluoropolymer interlayer avoids the direct exposure of the PEDOT:PSS surface to the basic developer and prevents any damage at the PEDOT:PSS/insulator interface. Fig. 5.2d and e show that the electrode

current noise in devices of type 3 was dramatically reduced down to 3 pA, a factor of 4 smaller compared with that in devices of type 1. In addition, there was a concomitant improvement in device-to-device reproducibility, as indicated by the small standard deviation. The reduced noise level in devices of type 3 improved drastically the signal-to-noise ratio during measurement of exocytotic events from a single chromaffin cell as shows in Fig. 5.2b-d.

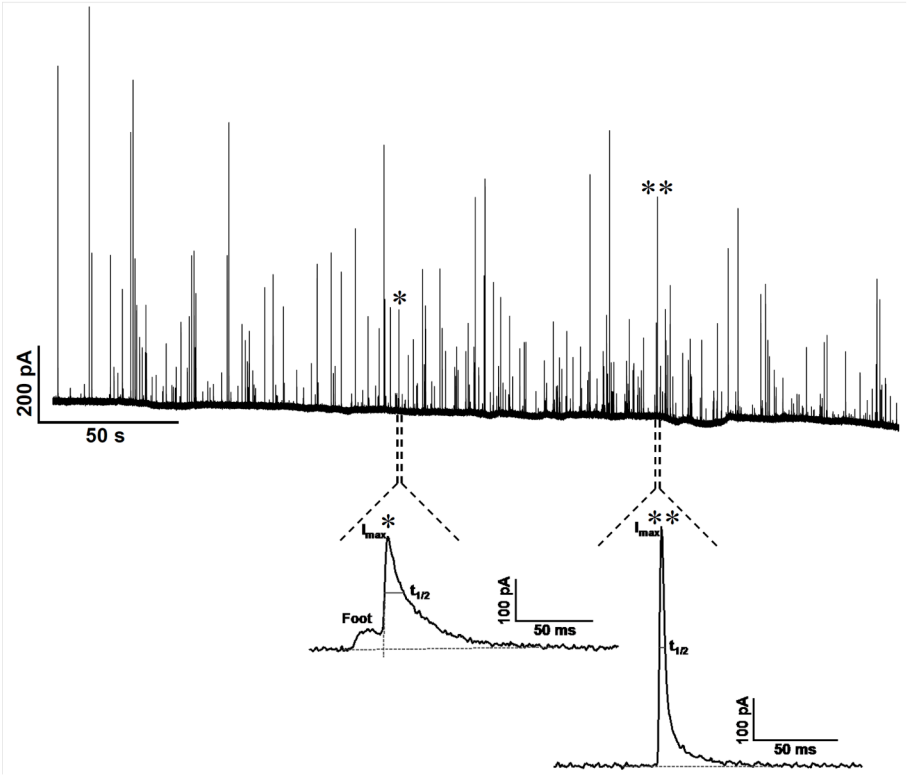

Figure 5.3. An amperometric trace recorded with a PEDOT:PSS microelectrode of type 3. The recording was obtained from a single chromaffin cell. Two individual amperometric spikes with (left) and without (right) a foot signal are shown on expanded time scale.

Fig. 5.3 shows an amperometric recording of transmitter release events from a single chromaffin cell placed on a PEDOT:PSS microelectrode of device type 3 in more detail. It also shows two amperometric spikes on expanded time scale. One of these shows a foot signal that reflects the slow flux of transmitter through the early narrow fusion pore. The amperometric spikes are typically quantified by determining

for each event the amperometric spike amplitude (I_{max}), indicating the maximum flux of catecholamines released from the vesicle, the spike width at half maximum ($t_{1/2}$) that is related to the kinetics catecholamine release from the vesicle, and the area under the spike obtained by integrating the current trace that provides the amperometric charge (Q_{amp}) which corresponds to the number of catecholamine molecules collected by the PEDOT:PSS microelectrode during an individual event. The duration of the foot signal indicates the time from the formation of a narrow fusion pore to its rapid expansion.

In addition to demonstrating the capability of PEDOT:PSS microelectrodes to monitor the time course of release of catecholamine transmitter from single vesicles, we quantified the amperometric spike characteristics measured with PEDOT:PSS microelectrodes of type 3. Fig. 5.4 shows a comparison with results obtained from Pt microelectrodes, which represent the state-of-the-art in planar microelectrodes for monitoring exocytosis. Nine cells each (N = 9) were tested, and a total of 1486 and 591 events were analyzed individually to determine amperometric spike parameters for PEDOT:PSS and Pt microelectrodes, respectively. It is worth noting that the mean of each parameter was determined for each cell and then, the parameters determined for each cell in a group were averaged to calculate the mean and the standard error of the mean (SEM) of a parameter [14]. The histograms in Fig. 5.4a and b show that the distribution of $t_{1/2}$ measured with PEDOT:PSS microelectrodes is similar to that measured with Pt microelectrodes. Also, the mean value of $t_{1/2}$ for PEDOT:PSS (8.39±1.05 ms; mean±SEM) was not significantly different from that for Pt (10.97±0.96 ms) as well as the reported mean values of $t_{1/2}$ for conventional CFEs, indicating that PEDOT:PSS microelectrodes correctly report the kinetics of quantal release events. In contrast, the mean Q_{amp} obtained with PEDOT:PSS microelectrodes (1.43±0.18 pC; mean±SEM) was about twice as large as that obtained with Pt microelectrodes (0.78±0.08 pC) with p=0.006 from a t-test (Fig. 5.4c and d).

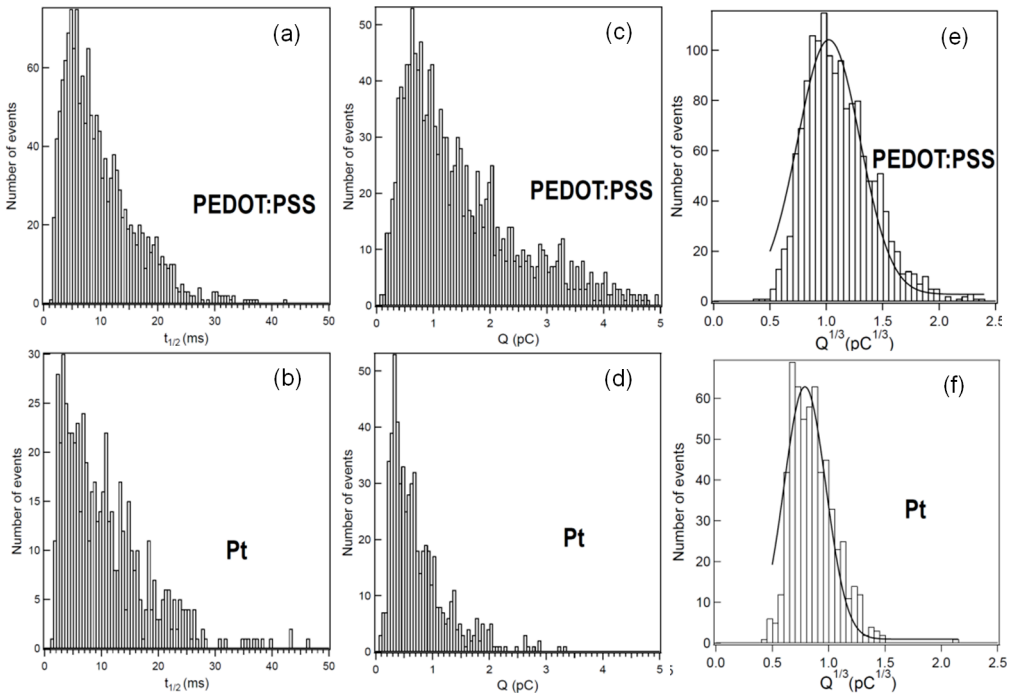

Figure 5.4. Analysis of amperometric spikes from chromaffin cell with PEDOT:PSS and Pt microelectrodes. Histograms represent the distribution of spike width at half maximum (a) and amperometric charge (c) for the PEDOT:PSS microelectrode. The distributions of spike width at half maximum and amperometric charge for the Pt microelectrode are shown in (b) and (d), respectively. The distribution of recorded quantal size was shifted to larger values for the PEDOT:PSS microelectrode. Spike widths are grouped in 0.5 ms bins and amperometric charge in 0.05 pC bins. Histograms of the cube root of amperometric charge measured with PEDOT:PSS (e) and Pt (f) microelectrodes. Solid lines are Gaussian fits.

At this point we can only speculate as to why the PEDOT:PSS microelectrodes collect almost twice as much charge as the Pt ones. A possible difference in the electrode area (e.g. assuming that the PEDOT:PSS microelectrode has higher surface roughness) cannot explain this observation: Since individual spikes are resolved, the current collected is limited by the inherent size of the vesicles and not by the electrode area. One explanation might involve the particular nature of charge transport in the PEDOT:PSS microelectrode: PEDOT:PSS is a degenerately doped p-type organic semiconductor, in which hole transport takes place within a fairly broad manifold of localized states arising from the highest occupied molecular orbitals that correspond to segments of the PEDOT chains [71]. The oxidation of catecholamine molecules de-dopes the surface of the PEDOT:PSS microelectrode and leaves a certain

number of sulfonate acceptors uncompensated. Steady-state is maintained through the injection of a hole current from the Pt lead, which re-dopes the microelectrode surface. Such de-doping and re-doping is known to change the position of the Fermi level inside the transport manifold, giving rise to a non-linear dependence of conductivity on dopant density [72]. Therefore, the variation in the current upon injection of a set number of electrons will be larger in PEDOT:PSS than in a metal electrode, in which the conductivity does not change with injected charge density.

It is worth noting that the frequency distribution of events measured by both PEDOT:PSS and Pt microelectrodes showed a Gaussian distribution when plotted as a function of $Q_{1/3}$, as seen in Fig. 5.4e and f, respectively. This is expected, as the distribution of vesicular radii in a chromaffin cell is Gaussian, and $Q_{1/3}$ is proportional to vesicular radius [5]. This result indicates that our analysis was based on the sufficient data collection, and that the PEDOT:PSS microelectrode provides a good means for monitoring secretion phenomena from chromaffin cells without distorting their nature.

Analysis of the foot signals provided a similar comparison between PEDOT:PSS and Pt microelectrodes. The mean foot duration of individual events and foot charge (integral of foot current) were 17.04±5.31 ms and 0.25±0.08 pC (mean±SEM, 28 of total 1486 events), respectively, when measured with PEDOT:PSS microelectrodes. The mean foot duration was 19.47±7.70 ms and the mean foot charge 0.10±0.04 pC (mean±SEM, 7 of total 591 events) when measured with Pt microelectrodes. Thus, while the same kinetics of fusion pore formation is obtained by both microelectrodes, the charge detected by the PEDOT:PSS microelectrodes is again about two-fold higher.

5.5. Conclusion and discussion

We demonstrated that PEDOT:PSS microelectrodes have the ability to detect transmitter release from single chromaffin cells during exocytosis. By optimizing the device architecture, microelectrodes were

fabricated that were able to record the oxidation of released catecholamines with a high signal-to-noise ratio. These microelectrodes accurately reported the kinetics of release and showed a two-fold increase in the amount of detected charge compared to planar Pt microelectrodes. The detection of transmitter release from living cells represents a new capability for interfacing with the nervous system using organic electronics, and one that allows new bioelectronic devices to be envisioned. One example is the combination with organic electronic ion pumps, devices that control the release of neurotransmitters, to yield an all-organic artificial synapse.

5.6. Note to Chapter 5

This work was done in collaboration with the co-authors; Brian Kim designed the work and conducted the cell recordings as well as the data analysis; Sang Yoon Yang designed the work and fabricated PEDOT:PSS electrodes as well as the data analysis; Alexander A. Zakhidov, Priscilla G. Taylor, and Jin-Kyun Lee contributed in the design of PEDOT:PSS electrode; Christopher K. Ober, Manfred Lindau, and George G. Malliaras designed the work. Thanks are due to Quinghua Fang for helping with the cell culture. This work was performed in part at the Cornell NanoScale Science and Technology Facility (CNF). Financial support from the Cornell Nanobiotechnology Center, NIH grant R01-NS048826, the FlexEBio IGERT (NSF 0654112) and the Partners University Fund are acknowledged. The material in Chapter 5 has been published in Advanced Materials [47].

CHAPTER 6

CONCLUSIONS AND FUTURE DIRECTIONS

In this dissertation, microfabrication techniques were applied to improve and invent instrumentations for single-cell amperometry. A novel approach, post-fabrication of Integrated Circuit (IC), was introduced to simplify the production of high-throughput biosensors. An active CMOS-based electrochemical biosensor array with high throughput capability (100 electrodes) was able to measure neurotransmitter release on-chip. The biosensor was designed and fabricated using the combination of pre-fabrication IC chips and a post-IC photolithography process, called post-fabrication, to incorporate platinum working electrodes on-chip. The on-chip working electrodes were patterned by conformal deposition of Pt and lift-off photolithography. The conformal deposition method protected the underlying electronic circuits from possible contact with the electrolyte that covers the electrode array during measurement. The biosensor was capable of resolving small and fast amperometric spikes reporting release from individual vesicle secretions. The effect of L-dopa was revealed using IC biosensors and the experiment for two cell groups, the control and the L-dopa treated, took less than 20 minutes. We anticipate that this device will accelerate the characterization of the modulation of neurotransmitter secretion from neuronal and endocrine cells by pharmacological and molecular manipulations of the cells. For example, an anticonvulsant drug named Levetiracetam with an unknown molecular mechanism on the vesicle secretion can be studied using the method presented in this chapter, with a significantly less effort compared to using conventional CFE method. Despite the fact that many drugs including Levetiracetam have an unknown molecular effect on the transmitter release, they are used clinically. With the reduction in time and cost for the drug screening process using IC biosensors, the specific modifications of the transmitter release process that these drugs produce can be identified, leading to an understanding of the molecular mechanisms by which these drugs exert their clinical effects. The production yield of

photolithography-based post-fabrication is limited due to frequent mis-alignment during fabrication because IC dies are small pieces of silicone which cause an imperfect coating of photoresist. To improve the post-fabrication efficiency, an improved and alignment-free post-fabrication method named tape-off, which overcomes several disadvantages of photolithography-based post-fabrication, was therefore developed.. , The tape-off method was validated by creating an electrochemical detection IC sensor and electrochemically recording DA oxidation. The electrochemical array showed a stable baseline and successfully measured the oxidation of DA as well as the quantal release from chromaffin cells, proving the successful implementation of tape-off to IC biosensor. The tape-off technique can be used to pattern metal, but may also be used in conjunction with other materials including protein and polymer brushes such as poly-lysine, typically used to enhance cell adhesion. Because tape-off is a completely dry process unlike photolithography that introduces contacts to chemicals, such as photoresist, developer, and photoresist remover, tape-off could be useful in the patterning of biological substances and organic materials which can be easily damaged by the photolithography chemicals. Currently, in order to pattern biological or organic materials, micro-contact printing and the parylene peel-off are two commonly used techniques because they limit the contact of the pattern material to the harmful chemicals. Tape-off can be an alternative for this application and may show significant advantages over parylene peel-off or other biocompatible processes. Parylene peel-off (and most processes) is/are not a self-aligned pattern but rely on photolithography to pre-pattern of parylene. However, parylene peel-off cannot be repeated unless photolithography is repeated to pattern the parylene film. Micro-contacting printing uses polydimethylsiloxane (PDMS) as an image transfer media and the stamping of PDMS requires an alignment of PDMS to the pattern target surface to re-pattern the target material. Tape-off can be easily repeated in few minutes to result in a self-aligned pattern, once the permanent cavities have been defined and require a minimum or no equipment. This technique will be able to introduce a micro-pattern method for biological or organic materials to people who are not equipped with microfabrication equipment and expertise. The yield of tape-off is guaranteed when cavities with high aspect ratios (depth/width) are used.

With 10 μm width and 1.5 μm depth cavities, a success rate of 100% was achieved. Also, the material to pattern must be removable by tape-off. Some materials such as Ti or Al form a very strong bond on SiO_2 and Si substrate and cannot be removed by tape-off. In this case, tape-off cannot create a pattern because the material residing on neither recessed nor upper compartment is removed after tape-off.

USB-communicating ADCs were fabricated to operate and record IC biosensor with portability (154 cm^3). The portable device was able to record 0-5 V ranged analog data with 400 kS/s sampling rate through USB. Ten analog-to-digital converters (ADCs) were designed on the device to sample analog data with 12-bit resolution. Through a USB port, outputs from all ADCs were transmitted simultaneously without any data loss. A high throughput biosensor with 10 analog outputs was both operated by and recorded using this portable USB-ADC device. New software was developed to effectively record all the data and display a selected electrochemical recording while acquisition. This involved rapid demultiplexing of streaming data. Compared to commercially available recording setups of analog signals, the USB-ADC was very cost effective and was compatible with a portable laptop. The work in the chapter extended the concept of simplifying and lowering the cost for amperometric recording setups and added portability. The electrochemical recording for transmitter release, with the technique introduced in the chapter, no longer requires the expertise in handling the microscope, microelectrode micro-positioning to approach the cell, and in hardware and software setup for the signal amplification and data storage. But with the USB-ADC and IC biosensor presented, the single-cell amperometry is as simple as plugging in an USB connector and pressing a start button. The method to produce USB-ADC is not limited to amperometric recordings only and can simply be customized to produce general-purposed ADCs and serve as a portable ADC device for variety recording applications. In order to accommodate larger electrode arrays or IC biosensors with a faster sampling rate, the USB transmission must run at faster rates than 2 or 4 MHz that is used in the current device. The USB rate scales linearly with the sampling rate of the USB-ADC. A faster USB rate above 4 MHz can be accomplished by sacrificing the total duration of measurement. This is because the overflow of RAM occurs at certain point throughout the

recording when data becomes excessive. The time of RAM failure depends on each computer configuration and thus, the total duration of stable operation must be identified for each computer environment if USB rate above 4 MHz is used. Additionally, the USB-ADC sampling rate may be improved with the use of USB 3.0 which however will require a new software development.

Lastly, a conducting polymer, PEDOT:PSS, was used to detect transmitter release from living cells and was presented as organic electronics for interfacing with the nervous system. By optimizing the device architecture, microelectrodes fabricated was able to detect transmitter release from single chromaffin cells during exocytosis. It exhibited a high signal-to-noise ratio and accurately reported the kinetics of release and showed a two-fold increase in the amount of detected charge compared to planar Pt microelectrodes. The reason for two-fold increment in the quantal size detected maybe investigated by the use of chronoamperometry and is currently unknown. Using chronoamperometry, the number of transferred electrons per molecule can extracted precisely under a well-controlled experiment and can be compared to that of traditional electrochemical materials such as gold or platinum to identify the different electrochemical response of PEDOT:PSS. Whatever the mechanism is, the increased apparent quantal size makes PEDOT:PSS a promising material for measurements of quantal release with increased signal amplitude.

BIBLIOGRAPHY

[1] B. Alberts, D. Bray, J. Lewis, M. Raff, K. Roberts, and J. D. Watson, *Molecular Biology of the Cell*. New York: Garland Publishing, Inc., 1983.

[2] R. E. Coupland, *The Natural History of the Chromaffin Cell*. London: Longmans, Green and Co, 1965.

[3] D. Fasshauer, R. B. Sutton, A. T. Brunger, and R. Jahn, "Conserved structural features of the synaptic fusion complex: SNARE proteins reclassified as Q- and R-SNAREs," *Proceedings of the National Academy of Sciences,* vol. 95, pp. 15781-15786, December 22, 1998 1998.

[4] J. B. Sorensen, K. Wiederhold, E. M. Muller, I. Milosevic, G. Nagy, B. L. de Groot, H. Grubmuller, and D. Fasshauer, "Sequential N- to C-terminal SNARE complex assembly drives priming and fusion of secretory vesicles," *Embo J,* vol. 25, pp. 955-66, Mar 8 2006.

[5] L. W. Gong, G. Alvarez De Toledo, and M. Lindau, "Secretory vesicles membrane area is regulated in tandem with quantal size in chromaffin cells," *Journal of Neuroscience,* vol. 23, pp. 7917-7921, Aug 27 2003.

[6] Q. Fang, K. Berberian, L. W. Gong, I. Hafez, J. B. Sorensen, and M. Lindau, "The role of the C terminus of the SNARE protein SNAP-25 in fusion pore opening and a model for fusion pore mechanics," *Proc Natl Acad Sci U S A,* vol. 105, pp. 15388-92, Oct 7 2008.

[7] A. E. DOYLE, E. G. MCQUEEN, and F. H. SMIRK, "Treatment of Hypertension with Reserpine,with Reserpine in Combination with Pentapyrrolidinium,and with Reserpine in Combination with Veratrum Alkaloids," *Circulation,* vol. 11, pp. 170-181, February 1, 1955 1955.

[8] C. Montecucco and G. Schiavo, "Mechanism of action of tetanus and botulinum neurotoxins," *Mol. Microbiol.,* vol. 13, pp. 1-8, 1994.

[9] R. B. Sutton, D. Fasshauer, R. Jahn, and A. T. Brunger, "Crystal structure of a SNARE complex involved in synaptic exocytosis at 2.4 Å resolution," *Nature,* vol. 395, pp. 347-353, 1998.

[10] K. Kisler, B. N. Kim, X. Liu, K. Berberian, Q. Fang, C. J. Mathai, S. Gangopadhya, K. D. Gillis, and M. Lindau, "Transparent Electrode Materials for Simultaneous Amperometric Detection of Exocytosis and Fluorescence Microscopy," *J.Biomater. Nanobiotechnol.,* vol. 3, pp. 243-53, 2012.

[11] R. M. Wightman, J. A. Jankowski, R. T. Kennedy, D. T. Kawagoe, T. J. Schroeder, D. J. Leszczyszyn, J. A. Near, E. J. Diliberto jr., and O. H. Viveros, "Temporally resolved catecholamine spikes correspond to single vesicle release from individual chromaffin cells," *Proceedings of the National Academy of Sciences, USA,* vol. 88, pp. 10754-10758, 1991.

[12] R. H. Chow, L. v. Rüden, and E. Neher, "Delay in vesicle fusion revealed by electrochemical monitoring of single secretory events in adrenal chromaffin cells," *Nature,* vol. 356, pp. 60-63, 1992.

[13] A. Albillos, G. Dernick, H. Horstmann, W. Almers, G. Alvarez de Toledo, and M. Lindau, "The exocytotic event in chromaffin cells revealed by patch amperometry," *Nature,* vol. 389, pp. 509-12, Oct 2 1997.

[14] T. L. Colliver, E. J. Hess, E. N. Pothos, D. Sulzer, and A. G. Ewing, "Quantitative and statistical analysis of the shape of amperometric spikes recorded from two populations of cells," *J Neurochem,* vol. 74, pp. 1086-97, Mar 2000.

[15] I. Hafez, K. Kisler, K. Berberian, G. Dernick, V. Valero, M. G. Yong, H. G. Craighead, and M. Lindau, "Electrochemical imaging of fusion pore openings by electrochemical detector arrays," *Proc Natl Acad Sci U S A,* vol. 102, pp. 13879-84, Sep 27 2005.

[16] F. Heer, W. Franks, A. Blau, S. Taschini, C. Ziegler, A. Hierlemann, and H. Baltes, "CMOS microelectrode array for the monitoring of electrogenic cells," *Biosens Bioelectron,* vol. 20, pp. 358-66, Sep 15 2004.

[17] F. Heer, S. Hafizovic, T. Ugniwenko, U. Frey, W. Franks, E. Perriard, J. C. Perriard, A. Blau, C. Ziegler, and A. Hierlemann, "Single-chip microelectronic system to interface with living cells," *Biosens Bioelectron,* vol. 22, pp. 2546-53, May 15 2007.

[18] J. J. Pancrazio, P. P. Bey, Jr., A. Loloee, S. Manne, H. C. Chao, L. L. Howard, W. M. Gosney, D. A. Borkholder, G. T. Kovacs, P. Manos, D. S. Cuttino, and D. A. Stenger, "Description and demonstration of a CMOS amplifier-based-system with measurement and stimulation capability for bioelectrical signal transduction," *Biosens Bioelectron,* vol. 13, pp. 971-9, Oct 15 1998.

[19] B. D. DeBusschere and G. T. Kovacs, "Portable cell-based biosensor system using integrated CMOS cell-cartridges," *Biosens Bioelectron,* vol. 16, pp. 543-56, Sep 2001.

[20] J. Rothe, M. K. Lewandowska, F. Heer, O. Frey, and A. Hierlemann, "Multi-target electrochemical biosensing enabled by integrated CMOS electronics," *Journal of Micromechanics and Microengineering,* vol. 21, May 2011.

[21] S. Ayers, K. Berberian, K. D. Gillis, M. Lindau, and B. A. Minch, "Post-CMOS fabrication of Working Electrodes for On-Chip Recordings of Transmitter Release," *IEEE Trans Biomed Circuits Syst,* vol. 4, pp. 86-92, Apr 1 2010.

[22] P. T. Kissinger, J. B. Hart, and R. N. Adams, "Voltammetry in brain tissue--a new neurophysiological measurement," *Brain Res,* vol. 55, pp. 209-13, May 30 1973.

[23] E. N. Pothos, V. Davila, and D. Sulzer, "Presynaptic recording of quanta from midbrain dopamine neurons and modulation of the quantal size," *J Neurosci,* vol. 18, pp. 4106-18, Jun 1 1998.

[24] D. Bruns and R. Jahn, "Real-time measurement of transmitter release from single synaptic vesicles," *Nature,* vol. 377, pp. 62-65, 1995.

[25] R. H. Chow and L. v. Rüden, "Electrochemical Detection of Secretion from Single Cells," in *Single Channel Recording*, B. Sakmann and E. Neher, Eds., 2nd ed New York: Plenum Press, 1995, pp. 245-275.

[26] W. Van der Kloot and J. Molgo, "Quantal acetylcholine release at the vertebrate neuromuscular junction," *Physiological Reviews,* vol. 74, pp. 899-991, Oct 1994.

[27] J. M. Finnegan, K. Pihel, P. S. Cahil, L. Huang, S. E. Zerby, A. G. Ewing, R. T. Kennedy, and R. M. Wightman, "Vesicular quantal size measured by amperometry at chromaffin, mast, pheochromocytoma, and pancreatic β-cells," *Journal of Neurochemistry,* vol. 66, pp. 1914-1923, 1996.

[28] D. Bruns, D. Riedel, J. Klingauf, and R. Jahn, "Quantal release of serotonin," *Neuron,* vol. 28, pp. 205-20, Oct 2000.

[29] T. L. Colliver, S. J. Pyott, M. Achalabun, and A. G. Ewing, "VMAT-Mediated changes in quantal size and vesicular volume," *J Neurosci,* vol. 20, pp. 5276-82, 2000.

[30] L. W. Gong, G. A. de Toledo, and M. Lindau, "Exocytotic catecholamine release is not associated with cation flux through channels in the vesicle membrane but Na^+ influx through the fusion pore," *Nat Cell Biol,* vol. 9, pp. 915-922, Aug 2007.

[31] E. Pothos, M. Desmond, and D. Sulzer, "L-3,4-Dihydroxyphenylalanine increases the quantal size of exocytotic dopamine release in vitro," *Journal of Neurochemistry,* vol. 66, pp. 629-636, 1996.

[32] K. D. Kozminski, D. A. Gutman, V. Davila, D. Sulzer, and A. G. Ewing, "Voltammetric and pharmacological characterization of dopamine release from single exocytotic events at rat pheochromocytoma (PC12) cells," *Anal Chem,* vol. 70, pp. 3123-30, Aug 1 1998.

[33] M. Criado, A. Gil, S. Viniegra, and L. M. Gutierrez, "A single amino acid near the C terminus of the synaptosomeassociated protein of 25 kDa (SNAP-25) is essential for exocytosis in chromaffin cells," *Proc Natl Acad Sci U S A,* vol. 96, pp. 7256-61, Jun 22 1999.

[34] S. Ayers, K. D. Gillis, M. Lindau, and B. A. Minch, "Design of a CMOS Potentiostat Circuit for Electrochemical Detector Arrays," *IEEE Trans Circuits Syst I Regul Pap,* vol. 54, pp. 736-744, Apr 1 2007.

[35] T. D. Parsons, J. R. Coorssen, H. Horstmann, and W. Almers, "Docked granules, the exocytic burst, and the need for ATP hydrolysis in endocrine cells," *Neuron,* vol. 15, pp. 1085-96, Nov 1995.

[36] E. V. Mosharov and D. Sulzer, "Analysis of exocytotic events recorded by amperometry," *Nat Methods,* vol. 2, pp. 651-8, Sep 2005.

[37] K. Berberian, K. Kisler, Q. Fang, and M. Lindau, "Improved surface-patterned platinum microelectrodes for the study of exocytotic events," *Anal Chem,* vol. 81, pp. 8734-40, Nov 1 2009.

[38] Y. Lin, R. Trouillon, M. I. Svensson, J. D. Keighron, A. S. Cans, and A. G. Ewing, "Carbon-ring microelectrode arrays for electrochemical imaging of single cell exocytosis: fabrication and characterization," *Analytical Chemistry,* vol. 84, pp. 2949-54, Mar 20 2012.

[39] T. J. Schroeder, J. A. Jankowski, K. T. Kawagoe, R. M. Wightman, C. Lefrou, and C. Amatore, "Analysis of diffusional broadening of vesicular packets of catecholamines

released from biological cells during exocytosis," *Analytical Chemistry,* vol. 64, pp. 3077-3083, 1992.

[40] J. Yao and K. D. Gillis, "Quantification of noise sources for amperometric measurement of quantal exocytosis using microelectrodes," *Analyst,* vol. 137, pp. 2674-81, Jun 7 2012.

[41] A. F. Dias, G. Dernick, V. Valero, M. G. Yong, C. D. James, H. G. Craighead, and M. Lindau, "An electrochemical detector array to study cell biology on the nanoscale," *Nanotechnology,* vol. 13, pp. 285-289, 2002.

[42] K. Berberian, K. Kissler, Q. Fang, and M. Lindau, "Improved Nanofabricated Electrochemical Detector Arrays for Monitoring Exocytosis," *Biophys. J.,* vol. 94, p. 1295, February 1, 2008 2008.

[43] M. K. Zachek, P. Takmakov, B. Moody, R. M. Wightman, and G. S. McCarty, "Simultaneous decoupled detection of dopamine and oxygen using pyrolyzed carbon microarrays and fast-scan cyclic voltammetry," *Analytical Chemistry,* vol. 81, pp. 6258-65, Aug 1 2009.

[44] B. Zhang, K. L. Adams, S. J. Luber, D. J. Eves, M. L. Heien, and A. G. Ewing, "Spatially and temporally resolved single-cell exocytosis utilizing individually addressable carbon microelectrode arrays," *Anal Chem,* vol. 80, pp. 1394-400, Mar 1 2008.

[45] S. Barizuddin, X. Liu, J. C. Mathai, M. Hossain, K. D. Gillis, and S. Gangopadhyay, "Automated targeting of cells to electrochemical electrodes using a surface chemistry approach for the measurement of quantal exocytosis," *ACS Chem Neurosci,* vol. 1, pp. 590-597, Jul 1 2010.

[46] V. Carabelli, S. Gosso, A. Marcantoni, Y. Xu, E. Colombo, Z. Gao, E. Vittone, E. Kohn, A. Pasquarelli, and E. Carbone, "Nanocrystalline diamond microelectrode arrays fabricated on sapphire technology for high-time resolution of quantal catecholamine secretion from chromaffin cells," *Biosens Bioelectron,* vol. 26, pp. 92-8, Sep 15 2010.

[47] S. Y. Yang, B. N. Kim, A. A. Zakhidov, P. G. Taylor, J. K. Lee, C. K. Ober, M. Lindau, and G. G. Malliaras, "Detection of transmitter release from single living cells using conducting polymer microelectrodes," *Adv Mater,* vol. 23, pp. H184-8, Jun 24 2011.

[48] J. Zhang, Y. Huang, N. Trombly, C. Yang, and A. Mason, "Electrochemical array microsystem with integrated potentiostat," in *Sensors, 2005 IEEE*, 2005, pp. 385-388.

[49] L. Li, X. W. Liu, W. A. Qureshi, and A. J. Mason, "CMOS Amperometric Instrumentation and Packaging for Biosensor Array Applications," *Ieee Transactions on Biomedical Circuits and Systems,* vol. 5, pp. 439-448, Oct 2011.

[50] P. Kruppa, A. Frey, I. Kuehne, M. Schienle, N. Persike, T. Kratzmueller, G. Hartwich, and D. Schmitt-Landsiedel, "A digital CMOS-based 24x16 sensor array platform for fully automatic electrochemical DNA detection," *Biosens Bioelectron,* vol. 26, pp. 1414-9, Dec 15 2010.

[51] R. M. Wightman, T. J. Schroeder, J. M. Finnegan, E. L. Ciolkowski, and K. Pihel, "Time course of release of catecholamines from individual vesicles during exocytosis at adrenal medullary cells," *Biophysical Journal,* vol. 68, pp. 383-390, 1995.

[52] X. Liu, S. Barizuddin, W. Shin, C. J. Mathai, S. Gangopadhyay, and K. D. Gillis, "Microwell device for targeting single cells to electrochemical microelectrodes for high-throughput amperometric detection of quantal exocytosis," *Analytical Chemistry,* vol. 83, pp. 2445-51, Apr 1 2011.

[53] M. K. Zachek, P. Takmakov, J. Park, R. M. Wightman, and G. S. McCarty, "Simultaneous monitoring of dopamine concentration at spatially different brain locations in vivo," *Biosens Bioelectron,* vol. 25, pp. 1179-85, Jan 15 2010.

[54] I. Palchetti and M. Mascini, "Electroanalytical biosensors and their potential for food pathogen and toxin detection," *Anal Bioanal Chem,* vol. 391, pp. 455-71, May 2008.

[55] P. Arora, A. Sindhu, N. Dilbaghi, and A. Chaudhury, "Biosensors as innovative tools for the detection of food borne pathogens," *Biosens Bioelectron,* vol. 28, pp. 1-12, Oct 15 2011.

[56] B. N. Kim, A. D. Herbst, S. J. Kim, B. A. Minch, and M. Lindau, "Parallel recording of neurotransmitters release from chromaffin cells using a 10×10 CMOS IC potentiostat array with on-chip working electrodes," *Biosensors and Bioelectronics,* vol. 41, pp. 736-744, 2013.

[57] R. S. Kane, S. Takayama, E. Ostuni, D. E. Ingber, and G. M. Whitesides, "Patterning proteins and cells using soft lithography," *Biomaterials,* vol. 20, pp. 2363-2376, 1999.

[58] J. Del Castillo and B. Katz, "La base "quantale" de la transmission neuromusculaire," *Colloques Internat. C.N.R.S. ,* vol. 67, pp. 245-256, 1957.

[59] R. M. Wightman, "Detection technologies. Probing cellular chemistry in biological systems with microelectrodes," *Science,* vol. 311, pp. 1570-4, Mar 17 2006.

[60] X. Sun and K. D. Gillis, "On-chip amperometric measurement of quantal catecholamine release using transparent indium tin oxide electrodes," *Anal Chem,* vol. 78, pp. 2521-5, Apr 15 2006.

[61] C. Amatore, S. Arbault, F. Lemaitre, and Y. Verchier, "Comparison of apex and bottom secretion efficiency at chromaffin cells as measured by amperometry," *Biophys Chem,* vol. 127, pp. 165-71, May 2007.

[62] C. Amatore, S. Arbault, Y. Chen, C. Crozatier, F. Lemaitre, and Y. Verchier, "Coupling of electrochemistry and fluorescence microscopy at indium tin oxide microelectrodes for the analysis of single exocytotic events," *Angew Chem Int Ed Engl,* vol. 45, pp. 4000-3, Jun 12 2006.

[63] M. Berggren and A. Richter-Dahlfors, "Organic bioelectronics," *Advanced Materials,* vol. 19, pp. 3201-3213, Oct 2007.

[64] R. M. Owens and G. G. Malliaras, "Organic Electronics at the Interface with Biology," *Mrs Bulletin,* vol. 35, pp. 449-456, Jun 2010.

[65] D.-H. Kim, S. Richardson-Burns, L. Povlich, M. R. Abidian, S. Spanninga, J. Hendricks, and D. C. Martin, "Soft, Fussy and Bioactive Conducting Polymers for Improving the Chronic Performance of Neural Prosthetic Devices," in *Indwelling Neural Implants: Strategies for Contending with the In Vivo Environment*, W. M. Reichert, Ed., ed Boca Raton: CRC Press, 2007, p. 177.

[66] J. Isaksson, P. Kjall, D. Nilsson, N. D. Robinson, M. Berggren, and A. Richter-Dahlfors, "Electronic control of Ca2+ signalling in neuronal cells using an organic electronic ion pump," *Nat Mater,* vol. 6, pp. 673-9, Sep 2007.

[67] D. T. Simon, S. Kurup, K. C. Larsson, R. Hori, K. Tybrandt, M. Goiny, E. W. Jager, M. Berggren, B. Canlon, and A. Richter-Dahlfors, "Organic electronics for precise delivery of neurotransmitters to modulate mammalian sensory function," *Nat Mater,* vol. 8, pp. 742-6, Sep 2009.

[68] Z. Zhou, S. Misler, and R. H. Chow, "Rapid fluctuations in transmitter release from single vesicles in bovine adrenal chromaffin cells," *Biophysical Journal,* vol. 70, pp. 1543-1552, 1996.

[69] J. Hwang, F. Amy, and A. Kahn, "Spectroscopic study on sputtered PEDOT center dot PSS: Role of surface PSS layer," *Organic Electronics,* vol. 7, pp. 387-396, Oct 2006.

[70] P. C. Taylor, J. K. Lee, A. A. Zakhidov, M. Chatzichristidi, H. H. Fong, J. A. DeFranco, G. C. Malliaras, and C. K. Ober, "Orthogonal Patterning of PEDOT:PSS for Organic Electronics using Hydrofluoroether Solvents," *Advanced Materials,* vol. 21, pp. 2314-+, Jun 2009.

[71] G. Malliaras and R. Friend, "An organic electronics primer," *Physics Today,* vol. 58, pp. 53-58, May 2005.

[72] J. Mort, S. Grammatica, D. J. Sandman, and A. Troup, "CHEMICAL CONTROL OF CONDUCTIVITY IN A MOLECULARLY-DOPED POLYMER," *Journal of Electronic Materials,* vol. 9, pp. 411-418, 1980.